Dyrk1a gene dosage in glutamatergic neurons has key effects in cognitive deficits observed in mouse models of MRD7 and Down syndrome

Authors

Véronique **Brault**[1], Thu Lan **Nguyen**[1], Javier **Flores-Gutiérrez**[1], Giovanni **Iacono**[2], Marie-Christine **Birling**[3], Valérie **Lalanne**[3], Hamid **Méziane**[3], Antigoni **Manousopoulou**[4,&], Guillaume **Pavlovic**[3], Loïc **Lindner**[3], Mohammed **Selloum**[1], Tania **Sorg**[1], Eugene **Yu**[5], Spiros D. **Garbis**[4,&] and Yann **Hérault**[1,3*]

Affiliations

[1] Université de Strasbourg, CNRS, INSERM, Institut de Génétique et de Biologie Moléculaire et Cellulaire, IGBMC, 1 rue Laurent Fries, 67404 Illkirch, France

[2]Department of Molecular Biology, Radboud Institute for Molecular Life Sciences, Radboud University, Nijmegen, the Netherlands.

[3] CELPHEDIA, PHENOMIN Université de Strasbourg, CNRS, INSERM, Institut Clinique de la Souris, 1 rue Laurent Fries, 67404 Illkirch, France

[4]Institute for Life Sciences, University of Southampton, School of Medicine, Southampton, UK;

[&] Current Address: Proteas Bioanalytics Inc., BioLabs at The Lundquist Institute, Torrance, 90502 CA, USA.

[5] The Children's Guild Foundation Down Syndrome Research Program, Genetics and Genomics Program and Department of Cancer Genetics and Genomics, Roswell Park Comprehensive Cancer Center, Buffalo, NY, USA; Genetics, Genomics and Bioinformatics Program, State University of New York At Buffalo, Buffalo, NY, USA.

***Corresponding author: Yann Hérault**

Phone: +33 388655657

Fax: +33 388655690

E-mail: herault@igbmc.fr

Keywords: DYRK1A, Down syndrome, MRD7, mouse models, glutamatergic neurons, memory

Abstract

Perturbation of the excitation/inhibition (E/I) balance leads to neurodevelopmental diseases including to autism spectrum disorders, intellectual disability, and epilepsy. Mutation in the *DYRK1A* gene located on human chromosome 21 (Hsa21) leads to an intellectual disability syndrome associated with microcephaly, epilepsy, and autistic troubles (MRD7). Overexpression of DYRK1A, on the other hand, has been linked with learning and memory defects observed in people with Down syndrome (DS). *Dyrk1a* is expressed in both glutamatergic and GABAergic neurons, but its impact on each neuronal population has not yet been elucidated. Here we investigated the impact of *Dyrk1a* gene copy number variation in glutamatergic neurons using a conditional knockout allele of *Dyrk1a* crossed with the Tg(Camk2-Cre)4Gsc transgenic mouse. We explored this genetic modification in homozygotes, heterozygotes and combined with the Dp(16*Lipi-Zbtb21*)1Yey trisomic mouse model to unravel the consequence of *Dyrk1a* dosage from 0 to 3, to understand its role in normal physiology, and in MRD7 and DS. Overall, *Dyrk1a* dosage in glutamatergic neurons did not impact locomotor activity, working memory or epileptic susceptibility, but revealed that *Dyrk1a* is involved in long-term explicit memory. Molecular analyses pointed at a deregulation

of transcriptional activity through immediate early genes and a role of DYRK1A at the glutamatergic post-synapse by deregulating and interacting with key post-synaptic proteins implicated in mechanism leading to long-term enhanced synaptic plasticity. Altogether, our work gives important information to understand the action of DYRK1A inhibitors and have a better therapeutic approach.

Author summary

The Dual Specificity Tyrosine Phosphorylation Regulated Kinase 1A, DYRK1A, drives cognitive alterations with increased dose in Down syndrome (DS) or with reduced dose in mental retardation disease 7 (MRD7). Here we report that specific and complete loss of *Dyrk1a* in glutamatergic neurons induced a range of specific cognitive phenotypes and alter the expression of genes involved in neurotransmission in the hippocampus. We further explored the consequences of *Dyrk1a* dosage in glutamatergic neurons on the cognitive phenotypes observed respectively in MRD7 and DS mouse models and we found specific roles in long-term explicit memory with no impact on motor activity, short-term working memory, and susceptibility to epilepsy. Then we demonstrated that DYRK1A is a component of the glutamatergic post-synapse and interacts with several component such as NR2B and PSD95. Altogether our work describes a new role of DYRK1A at the glutamatergic synapse that must be considered to understand the consequence of treatment targeting DYRK1A in disease.

Introduction

Down syndrome (DS; Trisomy 21), is the first genetic cause of mental retardation. The 21q22 contains a critical region (named DSCR for “Down syndrome Critical Region”) associated with most DS features including mental retardation. Among genes present in this region, the Dual-specificity Tyrosine-(Y)-phosphorylation-Regulated Kinase 1A (*DYRK1A*),

the mammalian homologue of the *Drosophila* minibrain (*mnb*) gene that is essential for normal neurogenesis, is a target for improvement of DS cognition [1]. In addition, Mental Retardation Disease 7 (MRD7) is caused by mutations, including loss-of-function, in *DYRK1A* [2-7], making this gene a critical dosage-sensitive gene for cognitive phenotypes.

The rodent *Dyrk1a* is expressed in foetal and adult brains in dividing neuronal progenitors and later in the adult cerebellum, olfactory bulb and hippocampus. DYRK1A is a serine/threonine kinase with substrates including transcription (CREB, NFAT, STAT3, FKRH), translation (ElF2Be) and splicing factors (SF2, SF3), protein regulating cell cycle (Cyclin B1 and B2) and apoptosis (Caspase 9, P53), synaptic proteins involved in endocytosis/exocytosis, intracellular trafficking, dynamic of the actin cytoskeleton (N-WASP), microtubule formation (MAP1B) and proteins implicated in inter cellular communication (NOTCH, GSK3b). Roles of DYRK1A have been revealed in brain development and neuronal differentiation via the control of critical signalling pathways such as AKT, MAPK/ERK and STAT3 or in synaptic function via the NFAT pathway [8, 9]. Transgenic mice with either excess or haploinsufficiency of *Dyrk1a* show cognitive deficits like those observed in patients with specific impairment of hippocampal-dependent learning and memory [10-12].

Among the mechanisms proposed to underlie the cognitive deficits in DS is glutamatergic and GABAergic neurotransmitter dysfunction. Studies of the DS mouse model Ts65Dn trisomic for about 56% of the human chromosome 21 (Hsa21) syntenic region on mouse chromosome 16 (Mmu16) have revealed excess GABAergic input leading to reduced activation of NMDA receptors and reduction of long-term potentiation (LTP) in the hippocampal CA1 and dentate gyrus (DG) areas [13]. In addition, enhanced hippocampal long-term depression (LTD) has also been observed in the hippocampi of Ts65Dn mice in response to sustained activation of excitatory synapses and attributed to excessive signalling via NMDA receptors [14-16]. Recent evidence supports the contribution of DYRK1A to changes in

glutamatergic neurotransmission, with a BAC transgenic mouse line overexpressing *Dyrk1a*, showing alterations in glutamatergic synaptic proteins and normalization of *Dyrk1a* in Ts65Dn mice improving synaptic plasticity, GABAergic/glutamatergic balance, learning and memory [17, 18]. *Dyrk1a* heterozygous knockout mice also present a reduction in the dendritic arborisation and the spine density of glutamatergic pyramidal neurons of the cerebral cortex and alterations in glutamatergic and GABAergic synaptic proteins.

In this context, we hypothesized that change in the dosage of *Dyrk1a* in glutamatergic neurons of the hippocampus and cortex of DS and MRD7 mouse models somehow alter their development and/or normal working in adult brain, leading to the cognitive deficits observed in DS or *Dyrk1a* haploinsufficiency models. Analysis of DYRK1A function in glutamatergic neurons using a knockout approach is not possible as its full KO is homozygote lethal [19]. Thus, we decided to change the gene dosage of *Dyrk1a* in glutamatergic neurons either in a disomic (inactivation of one or two copies of *Dyrk1a*) or trisomic (going back to two copies of *Dyrk1a*) context. We selected the Tg(Camk2a-Cre) transgene to target the Cre recombinase in glutamatergic neurons within the forebrain [20] and we used the Dp(16)1Yey trisomic mouse model (abbreviated as Dp1Yey) containing a segmental duplication of the 22.9 Mb *Lipi-Zfp295* region including *Dyrk1a*, to return to two copies of *Dyrk1a* in the glutamatergic neurons of the Dp1Yey. This model has the advantages to include 65% of Hsa21 mouse gene orthologs and to be devoid of the 50 DS-irrelevant trisomic genes that are present on the Ts65Dn mini chromosome [21]. Dp1Yey mice present defects in working memory, long-term episodic memory, and associative learning. In addition to those tests, we also tested the impact of *Dyrk1a* gene dosage on the mouse social behaviour as MRD7 patients display autistic traits.

Results

Dyrk1a is expressed in Camk2a-positive cells and its full inactivation in the glutamatergic neurons induces brain defects.

Dyrk1a is ubiquitously expressed in different neuronal cell populations of the brain but with regional differences: the protein level being higher in the olfactory bulb, cerebellar cortex, cortical structures and granular and pyramidal cell layers of the hippocampus [22]. We checked DYRK1A expression in adult glutamatergic neurons, by co-immunohistochemical localisation with an antibody against CAMK2A and DYRK1A. In the wild-type adult mouse, both proteins were found in pyramidal and granular neurons of the hippocampus and dentate gyrus and in neurons of the cortex (Figure 1A).

To better understand the function of DYRK1A in glutamatergic neurons we inactivated both copies of *Dyrk1a* using a conditional approach, to generate a full knock-out in those neurons. A floxed *Dyrk1a* allele (*Dyrk1a*^{cKO} allele) was designed such that exon 7 that codes for the serine/threonine protein kinase active site signature domain was flanked by two *loxP* sites (Figure 1B). We used the Tg(Camk2aCre)4Gsc transgene [20] to generate the *Dyrk1a*^{Camk2aCre} allele (shortened as *Dyrk1a*^{C}) and we checked the ability of the Cre to recombine the *Dyrk1a* floxed allele in *Dyrk1a*$^{Camk2aCre/Camk2aCre}$ (recombination of both *Dyrk1a*^{cKO} alleles with the Cre recombinase; noted here *Dyrk1a*$^{C/C}$) mice. The generation of the deleted allele was detected by PCR analysis exclusively in brain areas where *Camk2a* is expressed (Figure 1B). Quantification of *Dyrk1a* mRNA in different brain regions confirmed that *Dyrk1a* is expressed at different relative levels in brain subregions (Figure 1C). Nevertheless, decrease of the *Dyrk1a* transcripts was found in the hippocampus, cortex and thalamus/hypophysis but not in the cerebellum of *Dyrk1a*$^{C/C}$ mice (Figure 1C). Loss of the DYRK1A protein was confirmed in the hippocampus by Western blot analysis (Figure 1D) and

147 immunohistology (Figure 1E). This reduction was more evident within the pyramidal cell layers
148 of the CA1 and CA3 composed mostly of glutamatergic neurons.

149 We analysed the implication of DYRK1A in glutamatergic neurons by looking at brain
150 morphology and cognitive phenotypes. Brain weight was significantly decreased in *Dyrk1a*$^{C/C}$
151 mice compared to control mice (90% of the control weight; Figure 2A). Morphometric analysis
152 at Bregma -1.5 (Figure 2B) unravelled reduced surface area of the total brain surface in
153 *Dyrk1a*$^{C/C}$ mice (~88% of control; Figure 2C). The area of the hippocampus including the
154 cornus ammonis fields (CA1, CA2 and CA3) and dentate gyrus (DG) did not significantly differ
155 between the two genotypes (Figure 2D). We measured the thickness of the oriens layer at the
156 CA1, CA2 and CA3 levels, of the pyramidal layer at the CA1 level, of the radiatum layer, of
157 the CA1 and DG molecular layers and of the granular layer of the DG and did not find any
158 difference between control and *Dyrk1a*$^{C/C}$ mice (Supplementary figure 1A). We also counted
159 neurons within the CA1 and did not find any modification in the density of pyramidal neurons
160 (Supplementary figure 1B). Specific decrease in cortical thickness was observed at the level of
161 the dorsal motor cortex (~78% of controls, Figure 2E) and of the somatosensory cortex (~76%
162 of controls, Figure 2E) whereas decrease in thickness at the more ventral auditory cortex level
163 was not significant (Fig. 2E). Measurements of the thickness of different layers in the
164 somatosensory cortex (Figure 2F) indicate decrease in the thickness of molecular layer I,
165 external granular and pyramidal layers II/III, internal pyramidal layer V and internal
166 polymorphic layer VI (Figure 2G). Only the internal granular layer IV was found unchanged
167 (Figure 2G). To investigate how change in cellularity might relate to cortical thickness, we
168 counted the number of cells present in SSC layers II-III, V and VI. We found that cellular
169 density in layers II-III, V and VI was increased by about 30% in *Dyrk1a*$^{C/C}$ mice (Figure 2H)
170 with the total number of neurons unchanged between *Dyrk1a*$^{C/C}$ and controls, suggesting an
171 impact of *Dyrk1a* inactivation on cell morphology or tissue organization.

172

173 **Full *Dyrk1a* inactivation in the glutamatergic neurons impacts general behaviour and**
174 **cognition**

175 To analyse mouse behaviour in *Dyrk1a*$^{C/C}$ mice, we first focused our attention on
176 locomotor activity and exploratory activity. Measurement of horizontal, or vertical, locomotor
177 activity during circadian cycle did not differ in *Dyrk1a*$^{C/C}$ mice compared to control mice
178 (Supplementary figure 2A, B). The analysis of exploratory behaviour in a novel environment
179 (open field (OF) test) indicated normal locomotor activity for the *Dyrk1a*$^{C/C}$ mice
180 (Supplementary figure 2C) but their exploratory pattern was altered as they spent significantly
181 more time in the centre of the OF (Figure 3A), suggesting a decreased anxiety. This phenotype
182 was confirmed in the elevated plus maze with *Dyrk1a*$^{C/C}$ mice spending significantly more time
183 in the open arms than control mice (Figure 3B). In this test, *Dyrk1a*$^{C/C}$ mice were also more
184 active, visiting more arms than the control mice (Figure 3C). The locomotor performance was
185 assessed in the rotarod task. *Dyrk1a*$^{C/C}$ mice exhibited slightly better performance in this test
186 than their control littermates, with an increase in latency to fall, indicating that motor balance
187 is not affected in those mice (Figure 3D).

188 Impact of the loss of *Dyrk1a* in glutamatergic neurons on cognition was evaluated using
189 different memory tests. Working memory was assessed by recording spontaneous alternation
190 in the Y-maze. The percentage of alternation between the three arms was similar between
191 *Dyrk1a*$^{C/C}$ and control mice (Supplementary figure 2D) indicating a normal working memory
192 in both genotypes. In this test, the number of visited arms during the 5 min session was not
193 significantly different in the *Dyrk1a*$^{C/C}$ mice compared to the controls, although those mice
194 showed more variability (Supplementary figure 2E). Long-term explicit memory requiring the
195 hippocampus and related medial and temporal lobe structures was tested with the novel object
196 recognition test (NOR) with 24 hours delay. Although *Dyrk1a*$^{C/C}$ mice showed as much interest

exploring the objects during the presentation session (Figure 3E) and during the discrimination session (Figure 3F) compared to control animals, they did not make any difference between the two objects during the retention trial (Figure 3G) by contrast to control mice who spent significantly more time on the novel object compared to the familiar one. Thus, the NOR test unravelled a deficit in long-term explicit memory in the *Dyrk1a*$^{C/C}$ mice. Then, we tested associative learning using the contextual fear-conditioning test. During the habituation, mice showed the same basal level of freezing whatever their genotypes were (Figure 3H, Habituation). However, *Dyrk1a*$^{C/C}$ mice showed significantly less freezing than control mice during contextual discrimination, indicating poorer performance in contextual learning (Figure 3H, Context). During the cued learning, *Dyrk1a*$^{C/C}$ mice responded like control mice to the conditioned stimulus, indicating normal cued fear (Supplementary figure 2F). As decreased freezing could be due to a deficit in pain sensitivity rather than a deficit in memory, we tested the mice in the hot plate test. *Dyrk1a*$^{C/C}$ mice had a decreased latency to elicit a first response to noxious thermal stimulus, suggesting that they were more sensitive to pain than control mice (Figure 3I). As pain sensitivity was never tested in *Dyrk1a* knock-out heterozygous mice (shortened as *Dyrk1a*$^{+/-}$), we also tested those mice in the hot plate. We also found that those mice are more sensitive to pain (Figure 3J).

As in Human *DYRK1A* heterozygous mutations lead to autistic behaviour in MRD7, mouse sociability was investigated in this full inactivation of *Dyrk1a* in the glutamatergic neurons. We presented an empty cage and a cage containing a congener to the tested mouse and measured the time spent by the tested mouse to sniff either cage. Both *Dyrk1a*$^{C/C}$ and control mice showed social preference as they spent significantly more time sniffing the cage containing the congener than the empty cage (Supplementary figure 2G, Social preference). However, the total amount of time spent with their congener was decreased in *Dyrk1a*$^{C/C}$ mice compared to control mice whereas the time spent exploring the empty cage did not differ (Figure

3K). Preference for social novelty was tested by placing a new congener in the empty cage. Both genotypes spent significantly more time sniffing the cage containing the new congener compared to the cage with the familiar one (>60% of the time allocated for the new congener) (Supplementary figure 2H, Social novelty preference). There was also no significant difference in the total time control and transgenic animals spent sniffing both congeners (Supplementary figure 2I, Social contact).

Finally, as *DYRK1A* haploinsufficiency in human is causing epilepsy, we challenged the homozygous inactivation in *Dyrk1a*$^{C/C}$ and control mice with two different doses of the seizure-provoking agent pentylenetetrazol (PTZ) and the occurrence of myoclonic, clonic and tonic seizures was scored. At both 30 mg/kg (Supplementary figure 2J and 50 mg/kg (Supplementary figure 2K), *Dyrk1a*$^{C/C}$ susceptibility to seizure was similar to control mice. Altogether, those results indicate that *Dyrk1a* full inactivation in glutamatergic neurons does not increase susceptibility to PTZ-induced seizure.

Hence, *Dyrk1a* inactivation in glutamatergic neurons only impacts specific cognitive function such as explicit long-term memory, contextual fear memory and exploratory behavior while having no impact in others such as working memory, social behaviour and epileptic susceptibility.

Dyrk1a inactivation in the glutamatergic neurons lowers expression of genes involved in neurotransmission in the hippocampus, while enhancing expression of genes implicated in the regulation of transcription.

The hippocampus is a key structure in memory formation. Long-term object recognition memory analysed in the NOR test was shown to require interaction between the hippocampus and the perirhinal cortex [23-25] while contextual fear memory involves a neural circuit including the hippocampus, amygdala and medial prefrontal cortex [26]. Although we could

not detect any morphological defect in the hippocampus of *Dyrk1a*$^{C/C}$ mice, those mice are defective in both long-term recognition and contextual fear memories. To unravel the potential molecular mechanisms underlying the learning defects of *Dyrk1a*$^{C/C}$ mice, we performed genome-wide transcriptional profiling (RNA-seq) of *Dyrk1a*$^{C/C}$ and control mice in the hippocampus at postnatal day 30. Analysis of the RNA-seq exon reads (DEseq algorithm, P<0.025) identified 297 up-regulated and 257 down-regulated genes in *Dyrk1a*$^{C/C}$ compared with controls (Supplementary Table S1,). To determine the putative cell types associated with the deregulated genes, we compared the sets of up- and down-regulated genes with the markers of hippocampal cell types obtained from single cell RNA-seq [PMID: 25700174][PMID: 29273784] (see methods). As a result, up-regulated genes were predominantly enriched in oligodendrocyte-expressed genes (hypergeometric test, *bonferroni* corrected, P<3.4E-13) whereas down-regulated genes were enriched in neuronal markers (hypergeometric test, *bonferroni* corrected, pyramidal markers P<2.3E-4, interneuronal markers P<8.3E-3) (Supplementary Table S2). This decrease in neuronal markers expression is not reflected by a decrease in neuronal cells in the hippocampus as we did not observe a decrease in the thickness of the pyramidal cell layers or the DG granular cell layer, and did not find a deficit in the number of neurons within the CA1 of the *Dyrk1a*$^{C/C}$ hippocampus (Supplementary figure 1). Next, we performed GO enrichment analyses of the lists of up- and down-regulated genes with using a *Benjamini* cut-off of P < 0.05 (Table 1). The strongest enrichments for up-regulated genes were related to transcriptional regulation and DNA methylation. This category of genes did not have any overlap with the oligodendrocyte overexpressed genes at the exception of the SRY-related HMG-box transcription factor *Sox8* and we did not find any enriched specific function for the list of the oligodendrocyte markers that are up-regulated in *Dyrk1a*$^{C/C}$ hippocampi. We counted the number of Olig2+ cells in the corpus-callosum and found no difference between *Dyrk1a*$^{C/C}$ and control mice, suggesting that increased oligodendrocyte markers is not due to an increased

number of oligodendrocytes (Supplementary figure 3). Interestingly, among up-regulated genes, we found *Nr4a1 (Nurr77), Arc (Arg3.1), Npas4, Fos (cFos), Egr1 (Zif268) and Fosb*, six immediate-early genes (IEGs) encoding proteins involved in transduction signals that are induced in response to a wide variety of cellular stimuli and that are implicated in neuronal plasticity. Looking at known late response genes known to be activated by NPAS4 [27] in glutamatergic neurons, only three out of thirty-four (10%) of them were significantly deregulated in the hippocampus of *Dyrk1a*$^{C/C}$ compared to control mice (Supplementary Table S3), with *Fam198b* being up-regulated and *Csrnp1*and *Slc2a1* being down-regulated. Among target genes of NPAS4 shared between excitatory and inhibitory cells, four out of twelve (~30%) that we looked at were found deregulated in the hippocampus of *Dyrk1a*$^{C/C}$ compared to control mice (*Lmo2* and *Fosl2*, up-regulated; *Mylk* and *Nptx2*, down-regulated). Down-regulated genes found in the hippocampus transcriptome of *Dyrk1a*$^{C/C}$ mice were associated with presynaptic vesicle exocytosis, regulation of neurotransmitter levels and neuron projection, and pointed at a perturbation of chemical synaptic transmission via the deregulation of proteins involved in synaptic vesicle exocytosis. Particularly, genes coding for proteins of the SNARE complex (*Snap25*, *Stx1a*, *Napa* and *Napb*), regulating its activity (*Doc2b*, *Snph*) or implicated in vesicular synaptic cycle (*Anxa7*, *Amph*, *Syn2*, *Syngr1*) were found down-regulated in the hippocampus of *Dyrk1a*$^{C/C}$ mice. This complex is known to mediate synaptic vesicle docking and fusion with the presynaptic membrane during neuromediator release. The SNARE complex was recently found, also with NPAS4, as a common pathway misregulated in models of DS overexpressing DYRK1A (Duchon et al, HMG).

Behavioural defects are induced in *Dyrk1a*$^{C/+}$ mice while partial rescue of memory alterations is observed in Dp1Yey/*Dyrk1a*$^{C/+}$ mice.

We investigated the respective consequences of *Dyrk1a* dosage in glutamatergic neurons on the cognitive phenotypes observed respectively in MRD7 and DS mouse models. We analysed

mice heterozygous for the *Dyrk1a* knockout allele in glutamatergic neurons to investigate the implication of this gene in the cognitive phenotypes of MRD7. We also performed a rescue experiment consisting on the return to two copies of *Dyrk1a* in the glutamatergic neurons of Dp1Yey trisomic mice. For this, we compared animals carrying $Dyrk1a^{Camk2aCre/+}$ (noted $Dyrk1a^{C/+}$), Dp1Yey, and Dp1Yey/$Dyrk1a^{Camk2aCre/+}$ (noted Dp1Yey/$Dyrk1a^{C/+}$), with $Dyrk1a^{cKO/+}$ as controls in behavioural tests. Mouse locomotor behaviour was tested in the open-field (OF). $Dyrk1a^{C/+}$ mice did not show any significant difference in locomotor activity compared to controls. Surprisingly, whereas in our conditions Dp1Yey mice travelled the same total distance in the OF as control mice, Dp1Yey/$Dyrk1a^{C/+}$ mice travelled significantly more distance (Figure 4A), suggesting that those mice are hyperactive. The percentage of time spent by the mice in the centre of the open field arena did not differ between genotypes (Figure 4B), suggesting normal anxiety-related behaviour. Mice heterozygous for *Dyrk1a* in glutamatergic neurons presented the same behaviour as control mice, indicating that removing only one copy of *Dyrk1a* is not enough to trigger decreased anxiety, as observed in the complete knockout of *Dyrk1a* in glutamatergic neurons (Figure 4B vs Figure 3A). Analysis of working memory was done using the Y maze test. All the four groups of mice visited the same number of arms during the test, suggesting a normal locomotor activity (Supplementary figure 4A). On the other hand, Dp1Yey mice showed lower percentage of spontaneous alternation as compared to control mice (Figure 4C), confirming the phenotype already observed in previous studies [28] (Duchon and Herault, HMG). This decreased performance was not restored by *Dyrk1a* normalization in glutamatergic neurons (Figure 4C). Haploinsufficiency of *Dyrk1a* in those neurons, like the inactivation of the two copies of *Dyrk1a*, did not trigger any change in working memory (Figure 4C). We therefore also tested $Dyrk1a^{+/-}$ mice in the same test. $Dyrk1a^{+/-}$ animals showed the same activity (number of visited arms, Supplementary figure 4B) and the same level of

322 alternation as their wild-type littermates, indicating a normal working memory (Supplementary
323 figure 4C).
324 We further tested the mice in the NOR test for long term reference memory. Both control and
325 Dp1Yey/*Dyrk1a*$^{C/+}$ mice showed a significant preferential exploration of the novel object
326 during the retention trial (Figure 4E) whereas Dp1Yey and *Dyrk1a*$^{C/+}$ mice spent the same time
327 on the two objects (Figure 4E). The deficit of novel object exploration during the retention
328 phase in Dp1Yey and *Dyrk1a*$^{C/+}$ mice was not due to a lack of familiar object exploration during
329 the presentation phase as both genotypes showed similar exploration times than control mice
330 (Figure 4D). Only Dp1Yey/*Dyrk1a*$^{C/+}$ showed a slight decrease in object exploration compared
331 to control mice during the presentation phase mice (Figure 4D), but this did not impair their
332 retention capacity during the test phase. Hence, the deficit in object recognition in Dp1Yey
333 mice could be rescued by normalization of *Dyrk1a* copy number in glutamatergic neurons and
334 is also generated by the absence of one copy of the gene in the same neuronal cell line. In the
335 fear conditioning test, all genotypes showed more freezing during the context phase after
336 conditioning than during the habituation phase and no difference was observed between
337 genotypes in the context response (Supplementary figure 4D). In the sociability 3-chambers
338 test, all the four groups of mice showed preference for the cage containing the mouse rather
339 than the empty cage (Supplementary figure 4E). No difference was found between the four
340 groups in the total amount of time spent sniffing the cage containing the congener
341 (Supplementary figure 4F). Hence, by contrast to *Dyrk1a*$^{C/C}$ mice, *Dyrk1a*$^{C/+}$ mice do not
342 present decreased social exploratory behaviour. Dp1Yey mice did not spend significantly more
343 time with the novel mouse compared to the familiar one, indicating no preference for social
344 novelty (Figure 4F). This phenotype was rescued by returning to two copies of *Dyrk1a* in
345 glutamatergic neurons (Figure 4F). *Dyrk1a*$^{C/+}$ mice also showed preference for social novelty
346 (Figure 4F).

Hence, both increase in *Dyrk1a* copy number in glutamatergic neurons of trisomic mice and haploinsufficiency of *Dyrk1a* in glutamatergic neurons impact explicit memory supporting a key role of *Dyrk1a* in glutamatergic function as a modulator of explicit memory, but other functions probably require normalization of *Dyrk1a* in other cell types to be restored.

Proteomic analysis confirms the impact of *Dyrk1a* gene dosage on synaptic activity.

To examine the contribution of DYRK1A in molecular pathways linked to the cognitive phenotypes associated to T21 in the glutamatergic neurons, we performed proteomic profiling of the hippocampus of control, Dp1Yey, Dp1Yey/*Dyrk1a*$^{C/+}$ and *Dyrk1a*$^{C/+}$ mice. We identified 63 proteins that were up-regulated and 16 that were down-regulated in the hippocampi of Dp1Yey mice compared with controls. Among those, 40 of the up-regulated and 12 of the down-regulated proteins were back to control levels in Dp1Yey/*Dyrk1a*$^{C/+}$ hippocampi, while one up-regulated protein in Dp1Yey was down-regulated in Dp1Yey/*Dyrk1a*$^{C/+}$ and 4 down-regulated proteins in Dp1Yey were up-regulated in Dp1Yey/*Dyrk1a*$^{C/+}$ mice. We found 51 up-regulated and 7 down-regulated proteins in the hippocampus of *Dyrk1a*$^{C/+}$ mice. Eleven of those proteins (CAMK2A, ATP6V1C1, DPP3, ERGIC1, GPM6A, CENPV, RPS28, AGAP2, SNX6, ABCA1, BRK1) were also deregulated in Dp1Yey and back to normal level in Dp1Yey/*Dyrk1a*$^{C/+}$, suggesting that they are impacted by *Dyrk1a* copy number in glutamatergic neurons (Figure 5A and Supplementary Table S4). We performed GO enrichment analysis on the list of deregulated proteins using the ToppCluster website, selecting a Bonferroni cut-off of $P<0.05$. Enrichment analysis indicates that pathways and GO components that are mostly affected by *Dyrk1a* gene dosage are synaptic, dendritic and axonal components (Figure 5B-C; Supplementary Table S5). Normalization of *Dyrk1a* copy number in the glutamatergic neurons did not rescue specific pathways but had a more global effect with 50 to 80% of the proteins present in each Dp1Yey enriched GO returning to normal amount in Dp1Yey/*Dyrk1a*$^{C/+}$ mice

(Figure 5B). Interestingly, decreased *Dyrk1a* gene dosage was found to impact pre-synaptic proteins as observed in the transcriptome of *Dyrk1a*$^{C/C}$ hippocampi, whereas increased *Dyrk1a* gene dosage was associated with the post-synapse and growth cone (Figure 5C). Proteins enriched in the hippocampus of *Dyrk1a*$^{C/+}$ mice were linked to translational activity whereas increased *Dyrk1a* gene dosage was associated to ATPase activity (Figure 5C).

Interaction of DYRK1A with post-synaptic proteins

Behavioural and proteomic analyses suggest a direct impact of DYRK1A at the glutamatergic synapse. Previous work from our laboratory already demonstrated a role of DYRK1A at the presynapse by showing interaction of DYRK1A with SYN1, a neuronal phosphoprotein associating with the cytoplasmic surface of the presynaptic vesicles and tethering them to the actin cytoskeleton [29, 30], and with CAMK2 that was previously shown to phosphorylate SYN1 leading to the release of the vesicle pool [31-33]. Moreover, we also found that SYN1 was phosphorylated by DYRK1A on its S551 residue *in vitro* and *in vivo*, highlighting the role of DYRK1A in SYN1-dependent presynaptic vesicle trafficking [33]. CAMK2, deregulated in our proteomic analysis, is also present in the glutamatergic postsynapse and has a major role in the molecular cascade leading to LTP [34]. To investigate a potential role of DYRK1A at the postsynapse, we looked at DYRK1A protein interaction with CAMK2 and key proteins of the postsynaptic density complex (PSD), GLUN2B (NR2B), PSD95 and SYNGAP. We carried co-immunoprecipitation (co-IP) experiments with adult mouse brain lysates using antibodies against DYRK1A and these proteins and using GAPDH as a negative control. We found CAMK2A, NR2B and PSD95 present in the immunoprecipitates (IPs) of DYRK1A, while DYRK1A was found in the IPs of NR2B, PSD95 and SYNGAP (Figure 5D), showing that these proteins interact together.

Discussion

Complete *Dyrk1a* inactivation leads to early embryonic lethality with homozygous null *Dyrk1a* mice presenting drastic developmental growth delay with smaller brain vesicles, hindering the investigation of *Dyrk1a* function in the brain [19]. We therefore used a conditional knockout strategy to analyse *Dyrk1a* function in glutamatergic neurons. We found a significant reduction of about 10% of brain weight and size of $Dyrk1a^{C/C}$ mice compared to control animals. In comparison with $Dyrk1a^{+/-}$ mice that have 30% brain reduction [35] and consistent with postnatal expression of *Camk2a*, this suggest that microcephaly observed in MRD7 results from different impacts of DYRK1A on brain neurogenesis during embryonic and postnatal development, with $Dyrk1a^{C/C}$ brain revealing the impact of DYRK1A on postnatal neuronal morphogenesis. Indeed, the cortical size reduction that we observed was associated with increased cell density, as observed by Guedj and collaborators in $Dyrk1a^{+/-}$ mice [35] and suggesting a reduction of neuronal processes as observed in the neocortex of $Dyrk1a^{+/-}$ mice [12, 36, 37].

DYRK1A deficit in glutamatergic neurons resulted in specific impacts on mouse behaviour, learning and memory. $Dyrk1a^{C/C}$ mice were less anxious, spending more time in the centre of the OF and in the open arms of the EPM, and showed decreased freezing performance in the fear-related contextual test indicating an impact on emotional behaviour. Deficit in contextual fear behaviour might be attributed to a defective hippocampal-to-basolateral amygdala transmission as a result of either a deficit in glutamatergic projections or deficit in excitatory activity [38]. Change in emotional behaviour in $Dyrk1a^{C/C}$ mice is not the result of an intrinsic hyperactivity, as the mice did not present increased locomotor activity either spontaneous (circadian activity) or novelty induced (OF). Hence, contrary to the hypoactivity induced by full *Dyrk1a* haploinsufficiency [39], absence of DYRK1A in glutamatergic neurons does not impact mouse locomotor activity. Thermal pain sensitivity was altered in $Dyrk1a^{C/C}$

mice that were more sensitive to heat. This higher nociception response was also observed in *Dyrk1a*$^{+/-}$ mice, suggesting that DYRK1A has an impact on central processes involved in the control of pain sensitivity. The glutamatergic system takes part in the nociceptive circuits and activation of the expression of IEGs, whose expression was found increased in *Dyrk1a*$^{C/C}$ mice, has been shown to be part of long-term events triggered in neuroadaptation to pain in those circuits [40]. Interestingly, we and our collaborators observed a decreased in the expression of some of these IEGs (*Npas4*, *Arc*, *c-Fos* and *Fosb*) in the hippocampi of Tg(Dyrk1a) and of the trisomic mouse models Dp1Rhr and Ts65Dn [41] (Duchon et al). IEGs are also believed to be crucial in the formation of long-term memory which we also found impacted in *Dyrk1a*$^{C/C}$ and trisomic mice [42]. Moreover, our meta-analysis of the transcriptomic data of hippocampi from five DS mouse models carrying Mmu16 segmental duplications and a transgenic model overexpressing *Dyrk1a* revealed regulatory protein networks centred around six protein hubs, among which were DYRK1A itself and NPAS4 (Duchon et al.) *Npas4* is a neuron-specific gene and is present in both excitatory and inhibitory neurons, activating distinct programs of late-response genes promoting inhibition onto excitatory neurons and excitation on inhibitory neurons [27]. But we did not found major changes in the expression of late response genes targeted by NPAS4 (Supplementary Table S3) [27]. This could be due to experimental bias as the transcriptomic analysis was done using RNA extracts from whole hippocampi containing different cell populations. This heterogeneity can hinder glutamatergic-specific expression of the late-response genes. Even though IEGs are well known markers to measure neuronal activity during cognitive stimulation, their impact in cognitive processes affected in cognitive deficit disorders are unknown and we have no explanation for IEGs overexpression in the hippocampus of *Dyrk1a*$^{C/C}$ animals. In our analysis, IEG expression changes have been observed in “naïve” mice that were not subjected to any exercise or behavioural test. It would be therefore also interesting to analyse the expression of IEGs and late-response genes in the

447 mice after induction of neuronal activity, as it was explored for activation of Arc mRNA
448 transcription in pyramidal neurons of the CA1 region of the hippocampus in Ts65Dn mice [43].
449 In addition to transcriptional up-regulation, we also observed a down-regulation of genes for
450 proteins involved in neuron projection, reinforcing the conclusion of a defective synaptogenesis
451 in *Dyrk1a*$^{C/C}$ animals, and proteins involved in synaptic vesicle cycle, implicating DYRK1A in
452 neurotransmitter release. Among the deregulated genes, we found *Amphiphysin* (*Amph*), which
453 its protein is a known target of DYRK1A [44], and *Synapsin 2* (*Syn2*), which paralog
454 SYNAPSIN 1 was found to be hyperphosphorylated by DYRK1A overexpression in TgDyrk1a
455 mice [33]. Moreover, DYRK1A was found to phosphorylate MUNC18-1 [45], which interacts
456 with the SNARE complex protein Syntaxin 1A, whose transcripts are also decreased in the
457 hippocampus of *Dyrk1a*$^{C/C}$ mice and which was found to be one of the six hubs connecting the
458 major subnetwork biological cascades found deregulated in DS models (Duchon et al.). Our results
459 together with others [44, 46, 47] point at a role of DYRK1A in the glutamatergic presynapse in
460 the control of neurotransmitter release through synaptic vesicles exocytosis and vesicles
461 recycling processes.

462 We assessed the impact of *Dyrk1a* deficit in the glutamatergic neurons in *Dyrk1a*$^{C/+}$ as
463 a model of MRD7. While *Dyrk1a*$^{C/C}$ mice were less anxious, this phenotype was not observed
464 in *Dyrk1a*$^{C/+}$ mice, indicating that haploinsufficiency of *Dyrk1a* is not sufficient to trigger this
465 decreased anxiety pattern. Working memory was not affected neither in *Dyrk1a*$^{C/+}$ nor
466 *Dyrk1a*$^{C/C}$ mice. This fits with our observation that working memory is also not affected in
467 *Dyrk1a*$^{+/-}$ mice. We found that long-term recognition memory is affected in both *Dyrk1a*$^{C/+}$ and
468 *Dyrk1a*$^{C/C}$ mice. Deficit in long-term NOR has also been described in *Dyrk1a*$^{+/-}$ mice [12] and
469 in transgenic model overexpressing *Dyrk1a* alone [33] (DUCHON). Together with the rescue
470 of this type of memory in Dp1Yey, our findings show that DYRK1A has a direct cell-
471 autonomous function in regulating long-term explicit memory in glutamatergic neurons.

Cognitive deficits observed in DS have been linked to a perturbation of synaptic transmission due to defects in the control of the excitatory/inhibitory balance. In addition, most of the phenotypes observed in DS people and models are due to defects in the hippocampus or the prefrontal cortex [48]. Analysis of trisomic mouse models has revealed an overproduction of the inhibitory neurotransmitter GABA restricting synaptic activation of the glutamatergic NMDA receptors. Furthermore, *Dyrk1a* has been implicated in glutamate-GABA imbalance [49, 50]. However, how *Dyrk1a* controls the balance between the two pathways is still not clear. We performed a genetic rescue returning to two copies of *Dyrk1a* exclusively in cortical and hippocampal glutamatergic neurons of Dp1Yey mice and carried behavioural analysis of those mice to see if this rescue was enough to restore cognitive functions in Dp1Yey mice. We already found that Dp1Yey mice have deficits in both hippocampus-dependent spatial working and long-term explicit memory (Duchon et al.). In addition, Yu and collaborators showed deficits in hippocampal-mediated context memory [51]. We confirmed the deficit in in long-term explicit memory and in working memory. However, we did not observe a deficit in contextual memory in those mice. Normalization of gene copy number in glutamatergic neurons only partly restored the cognitive functions that were impacted in the Dp1Yey mice. Working memory deficit was not restored in Dp1Yey/*Dyrk1a*$^{C/+}$ mice. As *Dyrk1a* haploinsufficiency does not impact working memory, this could question the role of *Dyrk1a* in the deficit observed in Dp1Yey mice. Nevertheless, the overexpression of *Dyrk1a* alone was able to induce a deficit in spontaneous alternation [33] (DUCHON). Deletion of *Dyrk1a* under Camk2a-Cre occurs after birth and hence the lack of rescue of working memory in Dp1Yey/*Dyrk1a*$^{C/+}$ mice could result from prenatal brain defects. However, it was shown that spontaneous alternation in rodents is not present during the early postnatal stages of development (before postnatal day 30), indicating that brain processes sustaining this behaviour develops between the second and fourth postnatal week [52]. Furthermore, treatment of adult mice with an inhibitor of DYRK1A

is sufficient to restore working memory in Ts65Dn mice [50]. This lack of rescue presumably comes from the effect of *Dyrk1a* overexpression in non-glutamatergic neurons. The role of the GABAergic system on spontaneous alternation is not determined but the injection of a $GABA_A$ receptor agonist has been shown to decrease spontaneous alternation rates [53, 54]. Furthermore, DYRK1A was shown to act on GABA-producing enzymes [49]. Testing this hypothesis will require to normalize *Dyrk1a* in GABAergic neurons.

DS patients are affected in their explicit long-term memory abilities with a particular impairment in the visuo-perceptual processing [55]. We used the visual-object recognition NOR test as a paradigm to assess long-term explicit memory in the mouse. Both TgDyrk1a and Ts65Dn mouse models have been shown to have impaired long-term object recognition memory that could be ameliorated by treating the adult mice with the DYRK1A inhibitors [56-58]. We show here that correcting *Dyrk1a* gene copy number in glutamatergic neurons is sufficient to rescue explicit long-term memory in Dp1Yey/*Dyrk1a*$^{C/+}$ mice. Moreover, DYRK1A shortage in glutamatergic neurons is also sufficient to trigger long-term memory deficit. Hence *Dyrk1a* gene dosage seems to have an important role in glutamatergic neuronal defects observed in DS and MRD7 mouse models. TgDyrk1a mice have been shown to have bidirectional changes in synaptic strength with elevated LTP, reduced LTD [10] and dysregulated NMDA-receptor mediated calcium signalling [59]. Furthermore, normalization of *Dyrk1a* expression in the hippocampus of Ts65Dn mice can partially restore the deficit of LTP in the CA1 of Ts65Dn mice. As Dp1Yey mice show similar hippocampal LTP deficit [51], it would be interesting to see if *Dyrk1a* normalisation in the glutamatergic neurons could restore LTP in Dp1Yey/*Dyrk1a*$^{C/+}$ mice.

Excessive GABAergic inhibition has been proposed as the major cause of the perturbation between excitatory and inhibitory neurotransmission, with glutamatergic deficit being the consequence of over-inhibition of the NMDA receptors resulting in deficit of LTP

and memory [60]. Our finding outlines the glutamatergic deficit as a distinct alteration with *Dyrk1a* overexpression playing a key role in glutamatergic dysfunction and GABA-mediated over-inhibition combining with it to produce the full DS cognitive deficit. This also raises the question of the role of *Dyrk1a* overexpression in GABAergic neurons as other trisomic genes are also potential candidates for neuronal dysfunction. For example, overexpression of *Girk2* leads to increase in $GABA_A$-mediated GIRK currents in hippocampal neuronal cultures, affecting the balance between excitatory and inhibitory transmission [61, 62].

The finding of a cell-autonomous impact of DYRK1A in glutamatergic neurons on long-term memory function is supported by the impact of increased *Dyrk1a* gene dosage in glutamatergic neurons on the amount of glutamatergic post-synaptic proteins. Hence, among enriched proteins in the hippocampus of Dp1Yey mice that turned back to normal in the hippocampus of Dp1Yey/$Dyrk1a^{C/+}$ mice, we found CAMK2A, a subunit of the calcium/calmodulin-dependent protein kinase II (CAMK2) which plays a critical role in LTP by regulating ionotropic glutamate receptors at postsynaptic densities, GPM6A, a neuronal membrane glycoprotein involved in neuronal plasticity, regulation of endocytosis and intracellular trafficking of G-protein-coupled receptors [63], the GRM3 G-protein-coupled metabotropic glutamate receptor, DLG2, a member of the postsynaptic protein scaffold of excitatory synapses interacting with the cytoplasmic tail of NMDA receptors [64] and the intracellular calcium-binding protein CALB2 functioning as a modulator of neuronal excitability [65]. Previous work done in our laboratory found several proteins from the PSD that were hyperphosphorylated in mice with three copies of *Dyrk1a* (TgDyrk1a) [35] and dephosphorylated by TgDyrk1a mouse treatment with a DYRK1A inhibitor [33]. Among those proteins, the NR2B is a subunit of the glutamatergic postsynaptic NMDA receptor which play a pivotal role in excitatory synaptic transmission. This result was validated by our Co-IP experiments showing an interaction between DYRK1A and NR2B. NR2B subunits are

expressed in the neocortex and hippocampus [66-68]. NMDA receptors in the mature hippocampus consist of two NR1 subunits associated with either two NR2A, two NR2B or one of each subunits [69, 70] and different forms of synaptic plasticity have been associated to different types of NMDA receptors [71-73]. Hence, in addition to its interaction with the NR1/NR2A-type of receptors [74], we also point out an association with NR1/NR2B receptors. Moreover, interaction between DYRK1A and the PSD proteins PSD95, CAMK2 and SYNGAP, detected by coIP, strongly suggests a role of DYRK1A at the glutamatergic postsynapse. In addition, absence of the GLUR1 subunit of the AMPA receptor in the IP of DYRK1A indicates that DYRK1A interact most specifically with the NMDA-PSD complex. Altogether, this strongly suggests an implication of DYRK1A at the glutamatergic post-synapse, somehow supporting its involvement in long-term memory formation.

Taking advantage of a conditional allele for *Dyrk1a* inactivation, we were able to associate *Dyrk1a* gene dosage changes in glutamatergic neurons to specific cognitive phenotypes and molecular modifications and demonstrated a major impact of *Dyrk1a* dose change at the glutamatergic synapse on long-term explicit memory while no impact was observed for motor activity, short-term working memory and susceptibility to epilepsy. Further analysis of DYRK1A impact on other neurons, such as GABAergic ones, will be necessary to understand how DYRK1A perturbs the excitatory/inhibitory pathways, resulting in the full DS and MRD7 cognitive deficits.

Materials and Methods

Mouse lines

The Dp(16Lipi-Zbtb21)1Yey (Dp1Yey) line was created by Yu and collaborators [75] and bears a 22.6 Mb segmental duplication of the *Lipi-Zfp295* fragment of murine chromosome 16 syntenic to Hsa21 [51, 75]. The transgenic Tg(Camk2-Cre)4Gsc line [20, 76] expressing the Cre recombinase under the control of the Camk2a promoter to inactivate the targeted conditional knockout allele in glutamatergic neurons of the cortex and hippocampus after birth. The Dyrk1$^{tm1.ICS}$ conditional knockout (noted Dyrk1a cKO) was generated at the PHENOMIN-ICS (Institut Clinique de la Souris; Illkirch, France; www.phenomin.fr) in the frame of the Gencodys consortium (http://www.gencodys.eu/).The targeting vector was constructed as follows. A 1096 bps fragment encompassing exon 7 (ENSMUSE00001246185) was amplified by PCR (from BAC RP23-115D20 genomic DNA) and subcloned in an MCI proprietary vector. This MCI vector contains a LoxP site as well as a floxed and flipped Neomycin resistance cassette. A 3.8 kb fragment corresponding to the 3' homology arm and 4.1 kb fragment corresponding to the 5' homology arms were amplified by PCR and subcloned in step1 plasmid to generate the final targeting construct. The linearized construct was electroporated in C57BL/6N (B6N) mouse embryonic stem (ES) cells. After selection, targeted clones were identified by PCR using external primers and further confirmed by Southern blot with a Neo probe (5' and 3' digests) as well as a 5' external probe. Two positive ES clones were injected into BALB/cN blastocysts. Resulting male chimeras were bred with Flp deleter females previously backcrossed in a C57BL/6N [77] (PMID: 10835623). Germline transmission of the conditional allele was obtained (Figure 1B). The Flp transgene was segregated by a further breeding step. By combining the three different lines together, we obtained the following groups of mice for phenotyping analyses: Dp1Yey (trisomic, for the *Lipi-Zfp295* fragment containing the *Dyrk1a* gene), Dp1Yey/*Dyrk1a*$^{C/+}$ (trisomic for the *Lipi-Zfp295* fragment but containing

596 only two copies of *Dyrk1a* in glutamatergic neurons), *Dyrk1a*$^{C/+}$ (containing only one copy of
597 *Dyrk1a* in the glutamatergic neurons) and *Dyrk1a*$^{C/C}$ (knocked out for *Dyrk1a* in glutamatergic
598 neurons). Wild-type, *Dyrk1a*$^{cKO/+}$ and *Dyrk1a*$^{cKO/cKO}$ mice were used as disomic controls.
599 For the genotyping of the mice and identification of the *Dyrk1a* knockout allele in the
600 brain, genomic DNA was isolated from tail and different organ biopsies using the NaCl
601 precipitation technique. 50-100 ng of genomic DNA was used for PCR. Primers used for the
602 identification of each allele and size of PCR products are described in Figure 1 and
603 Supplementary Table S6. Details on the genotyping protocol used here are published [78].
604 The mice were housed in groups (2–4 per cage) and were maintained under specific
605 pathogen-free (SPF) conditions and were treated in compliance with the animal welfare policies
606 of the French Ministry of Agriculture 133 (law 87 848).
607

608 **Mouse RT droplet digital PCR (ddPCR)**

609 Total RNA was extracted from frozen brain tissues (cerebellum, cortex, striatum, hippocampus
610 and thalamus/hypothalamus) of five wt and four *Dyrk1a*$^{C/C}$ mice as described in Lindner *et al.*
611 2020 [79]. For ddPCR, all primers were designed and synthesized as described in Lindner *et al.*
612 2020 [79] excepting Universal Probe Library probe used to *Dyrk1a* mRNA which is provided
613 by Roche. *Dyrk1a* and *Hprt* primers and probes sequences are given in Supplementary Table
614 S6. RNA reverse transcription, droplet generation, PCR amplification, droplets quantification
615 and analysis are also described in Lindner *et al* 2020 [79]. We presented the results as a ratio
616 of the mean of *Dyrk1a* RNA transcript in *Dyrk1a*$^{C/C}$ tissue normalized to the mean of *Dyrk1a*
617 RNA transcript in wt tissue. Experiments were performed following dMIQE guidelines for
618 reporting ddPCR experiments (Supplementary Table S7) [79, 80].

619 **Western blot analysis**

Twenty-five microgram of total protein extracts from hippocampi (n=3 per genotype) were electrophoretically separated in SDS-polyacrylamide gels (10%) and transferred to a nitrocellulose membrane (100V, 2h at room temperature). Non-specific binding sites were blocked with 5% skimmed milk in Tween20 0.1% Tris buffer saline 1h at room temperature. Immunostaining was carried out with a mouse monoclonal anti-Dyrk1a (Abnova, H00001859-M01) and an anti-Gapdh antibodies (ThermoFisher, MA5-15738), followed by secondary anti-mouse IgG conjugated with horseradish peroxidase (DAKO). The immunoreactions were visualized by ECL chemiluminescence system (Amersham) with the Amersham Imager 600. Semi-quantitative analysis was performed using ImageJ software (W. Rasband, NIH; http://rsb.info.nih.gov/ij/).

Immunohistological analysis

Adult mice were deeply anesthetized with sodium pentobarbital and perfused intracardially with 30 ml PBS followed by 30 ml 4% paraformaldehyde in PBS. Brains were removed from the skull and immersed in the same fixative overnight. After rinsing with PBS, the brains were transferred into 70% ethanol until paraffin inclusion. For inclusion, brains were dehydrated and embedded in paraffin. Serial 10 µm sections were made with a microtome.

Brain sections were stained using the myelin-specific dye luxol fast blue and the Nissl staining cresyl violet. Briefly, brain sections were deparaffinised, rehydrated and incubated in 0.1% luxol fast blue (95% alcohol and 0.5% acetic acid) solution at room temperature overnight. After rinsing excess stain with 95% ethanol and deionized water, the slides were placed in 0.05% lithium carbonate solution for 10 seconds followed by 70% ethanol for 5 seconds. They were then rinsed in deionized water until the colourless grey matter contrasted with the blue-green white matter. Sections were then stained in 0.1% cresyl violet acetate solution for 5 minutes at 56°C in a water bath, rinsed in deionized water and quickly in 100%

ethanol. Sections were dried, cleared in histosol® (Shandon) and mounted in Eukitt® (Labonord).

Immunohistology was performed using a standard protocol. After deparaffinization, rehydration and antigen retrieval (10 mM citric acid, 0.05% Tween 20, pH6.0) for 45 min in a 94°C water bath, sections were incubated in a blocking solution (0.05% Tween20, 5% Horse serum) for 1 hour at room temperature. Sections were then incubated at 4°C overnight with the primary antibodies (Mouse anti-Dyrk1a: Abnova, Cat. N. H00001859-M01; Rabbit anti-Camk2a: Molecular probes, PA5-14315). After washing, sections were incubated with anti-Mouse and anti-Rabbit Alexa Fluor®546 or 488 secondary antibodies for detection. The sections were mounted with Mowiol mounting medium (0.1M Tris (pH8.5, 25% glycerol, 10% w/v Mowiol 4-88 (Citifluor)) containing DAPI (5 µg/ml) and images were acquired using Hamamatsu Nanozoomer 2.0 (Hamamatsu, Hamamatsu City, Japan) and a Leica Upright fluorescent microscope (Leica Microsystems, Heidelberg).

Immunohistochemistry was performed using a standard protocol. Briefly, antigen retrieval was performed by heating the slides in Tris/EDTA buffer (10 mM Tris Base, 1 mM EDTA, 0.05% Tween 20, pH 9.0) for 45 min in a 94°C water bath. Then, the sections were quenched in 0.3% oxygen peroxide solution for 20 min and blocked with 10% normal horse serum and 0.1% Triton X-100 in 1× PBS for 1 h at room temperature. The sections were incubated overnight at 4°C with a rabbit anti-Olig2 antibody (1:500, Santa Cruz sc-48817). which was detected by incubating the sections with secondary biotinylated antibodies (Life Technologies^{TM}) for 2 h at room temperature and then with an avidin-biotin complex at 37°C for 30 min. Dark coloration was developed with diaminobenzidine tetrahydrochloride and the sections were mounted with aqueous mounting medium (Faramount aqueous mounting medium, Dako®).

Morphometric analysis

Morphometric analysis was performed on three *Dyrk1a*$^{C/C}$ and three control mice based on the standard operating procedures for morphological phenotyping of the mouse brain using basic histology [81]. Surface and cortical thickness measurements as well as cell counting were conducted on scanned images using Hamamatsu Nanozoomer 2.0 from luxol fast blue/cresyl violet-stained sections around Bregma -1.5 mm (Paxinos adult mouse brain atlas, Franklin and Paxinos, 1997). TIFF files were opened in ImageJ with the following settings: 9 decimal places (using the panel Analyze/Set Measurements) and "cm" as unit length (using Analyze/Set Scale). The polygone selection tool was used to measure area and the straight line tool was selected to measure length. The thickness of the different cortical layers (layer I to layer VI) were estimated in the somatosensory cortex based on the shape and density of the neurons on these different layers. Cell count performed in the somatosensory cortex was done within a counting frame of 0.1 cm. Cell count performed in the CA1 was done within a counting frame of 0.04 cm width). Olig2+-positive cells within the corpus callosum were counted by measuring a distance of 1 mm from the midline of the brain and selecting the corpus callosum area underneath. Cell count was done manually.

RNA-seq libraries and analysis

Total RNA was Trizol-extracted from 2 wild-type and 2 Dyrk1a$^{C/C}$ frozen P30 hippocampi. RNA was treated with DNase (Qiagen) and purified on the RNeasy MinElute Cleanup Kit (Qiagen). 2 µg of total RNA were treated with the Ribo-Zero rRNA Removal Kit (Human/Mouse/Rat; Illumina). Depleted RNA was precipitated 1h at -80°C in three volumes of ethanol plus 1 µg of glycogen. RNA was then washed and resuspended in 36 µl of RNAse free water. RNA fragmentation buffer (NEBNext® Magnesium RNA Fragmentation Module) was added to the solution and the RNA was fragmented by incubation at 95°C for 3 min. cDNA first strand synthesis was performed with random hexamer primers and cDNA second strand

695 synthesis was performed with dUTPs, to ensure strand specificity. The RNA-seq library was
696 synthetized with KAPA Hyper prep kit (Kapa Biosystems, Wilmington, MA, USA): a treatment
697 with USER enzyme (NEB, M5505L) was added to digest the unspecific strand.
698 The libraries were pooled (4/lane) on an Illumina HiSeq. 2000. Libraries were sequenced (50
699 cycles, single-end) yielding on average 40 million mapped reads. RNA-Seq libraries were
700 mapped with GSNAP (version 2015-06-23) against mm9 mouse RefSeq annotations updated
701 to the 28/7/2015.
702 DESeq 2 (v1.14) was used to perform statistical comparisons. All the enrichment analysis were
703 made from standard hypergeometric tests with benjamini or bonferroni correction. The markers
704 of hippocampal cell types were obtained from [ref] and the common background genes were
705 evaluated prior to the enrichment (hypergeometric test). GO annotations were updated to
706 25/6/2015.
707
708 **Proteomic analysis**
709 Fourty microgram of total protein extracts from hippocampus (4 controls, 5 Dp1Yey, 4
710 Dp1Yey; *Dyrk1a*$^{C/+}$ and 5 *Dyrk1a*$^{C/+}$) were used for the preparation. Samples were precipitated,
711 reduced, alkylated and digested with LysC and trypsin at 37°C overnight. 10 µg of each sample
712 were then labeled with TMT isobaric tags, pooled, desalted on a C18 spin-column and dried on
713 a speed-vacuum before nanoLC-MS/MS analysis. Samples were separated on a C18 Accucore
714 nano-column (75 µm ID x50 cm, 2.6 µm, 150 Å, Thermo Fisher Scientific) coupled in line with
715 an Orbitrap ELITE mass spectrometer (Thermo Scientific, San Jose, California). Samples were
716 analyzed in a Top15 HCD (High Collision Dissociation) mass spectrometry on 8h gradient.
717 Data were processed by database searching using SequestHT (Thermo Fisher Scientific) with
718 Proteome Discoverer 1.4 software (Thermo Fisher Scientific) against a mouse Swissprot
719 database (release 2015-03). Peptides were filtered at 5% false discovery rate (FDR) and one

peptide in rank 1. Protein quantitation (ratio of the intensity of the fragmented tag in sample "x" to the intensity of the fragmented tag in one control (disomic) sample used as the reference) was performed with reporter ions quantifier node in Proteome Discoverer 1.4 software with integration tolerance of 20 ppm, and the purity correction factor were applied according to the manufacturer's instructions. A scaling factor normalization method was used in order to make sample ratios comparable. Ratios were normalized by calculating the mean of all the peptide ratios in one sample, calculating a scaling factor (sf=mean [ratio control ref]/mean [ratio sample x]) for each sample and multiplying each ratio by the sf. Data were filtered with the following criteria: minimum number of peptide ratios used to calculate the protein ratio equal to 2 ; variability of the peptide ratios <20%; ratio of Dp1Yey and *Dyrk1a*$^{C/+}$ samples compared to mean of disomic controls, x>1.2 or x<0.8 and ratio of Dp1Yey;*Dyrk1a*$^{C/+}$ samples compared to mean of disomic controls 0.8<x<1.2 among proteins that were selected as deregulated in Dp1Yey. GO enrichment was calculated in the ToppCluster website (https://toppcluster.cchmc.org/), looking at enrichment within the following features: Molecular functions, Biological processes, Cellular components, Phenotypes and Pathways, and using a Bonferroni correction cut-off of P<0.05. The results of the enrichments can be found in the Supplementary Table, Excel File S5.

Co-immunoprecipitation

Immunoprecipitations were performed on fresh half brains of 3-month old wild-type male mice. Brains were dissected and lysed in 1.2 ml RIPA lysis buffer (Santa-Cruz Biotechnology, France) using Precellys® homogenizer tubes. After centrifugation at 2800 g for 2×15 s, 1 ml brain extract was incubated with 2 µg of antibody of interest at 4°C for 1 h under gentle rotation. An aliquot of the remaining supernatant was kept for further immunoblotting as homogenate control. Then, 20 µl protein G agarose beads, previously washed three times with bead buffer,

were added to the mix and gently rotated at 4°C for 30 min. After a 1 min spin at 10,000 g and removal of the supernatant, the pelleted immune complexes were washed three times with bead buffer before WB analysis with appropriate antibodies directed against DYRK1A (H00001859 M01, Interchim; 1:1000), NMDAR2B (Abcam, #ab65783), PSD95 (ab18258, Abcam, France; 1:1000), CAMK2A (PA5-14315, Thermo Fisher Scientific; 1:1000), SYNGAP (sc-8572, Santa Cruz biotechnologies; 1:5000) and GAPDH (MA5-15738, Thermo Fisher Scientific; 1:3000). Immunoblots were revealed with Clarity Western ECL Substrate (Bio-Rad).

Mouse behavioural analysis

A series of behavioural experiments were conducted in mice with a range of age starting at 2,5 up to 7 months, as described in the Supplementary information. For all these tests, mice were kept in ventilated cages with free access to food and water. The light cycle was controlled as 12 h light and 12 h dark (lights on at 7:00 AM) and the tests were conducted between 8:00 AM and 4:00 PM. Due to the difficulty to obtain Dp1Yey*; Dyrk1a*$^{KO/+}$ mice (triple crossing and subfertility of the Dp1Yey line), both males and females were pooled for the analysis. Animals were transferred to the experimental room 30 min before each experimental test. Behavioural experimenters were blinded as to the genetic status of the animals. Behavioural experiments were performed in agreement with the EC directive 2010/63/UE86/609/CEE and was approved by the local animal care, use and ethic committee of the IGBMC (Com'Eth, no.17, APAFIS 2012-069). The PTZ-induced seizures protocol received the accreditation number APAFIS#6321. All the standard operating procedures for behavioural phenotyping have been already described [82-84] and are detailed in the supplementary information.

Statistical analysis

769 Statistical analyses were performed using SigmaPlot software. For histological assessments and
770 behavioral tests comparing *Dyrk1a*$^{Camk2aCre/Camk2aCre}$ animals to controls, statistical analyses
771 were performed using unpaired t-test when appropriate or the non-parametric Mann-Whitney
772 rank sum test unless otherwise stated in the text. For the four groups analyses (Dp1Yey,
773 Dp1Yey; *Dyrk1a*$^{C/+}$, Dp1Yey, *Dyrk1a*$^{C/+}$and controls) a two-way ANOVA did not
774 reveal a significant effect of sex and no interaction with the genotype. Therefore, the sex factor
775 was dropped from the model and a one-way ANOVA and *post hoc* Tukey's multiple
776 comparison test were used to analyse differences between the four genotype groups.

Acknowledgments

We would like to thank members of the research group, of the IGBMC laboratory and of the ICS. We are grateful to the IGBMC proteomic plateform and Doulaye Dembele for their expert technical assistance in proteomic analysis, and Binnaz Yalcin and Stephan Collins for their help in brain morphometric analysis. We extend our thanks to the animal care-takers of the ICS who oversee the mice wellness.

This work has been supported by the National Centre for Scientific Research (CNRS), the French National Institute of Health and Medical Research (INSERM), the University of Strasbourg (Unistra), the French state funds through the “Agence Nationale de la Recherche” under the frame programme Investissements d’Avenir [ANR-10-IDEX-0002-02, ANR-10-LABX-0030-INRT, ANR-10-INBS-07 PHENOMIN to YH]. This project has received funding from the Jérôme Lejeune foundation and the European Union’s Horizon 2020 research and innovation programme under grant agreement No 848077. The funders had no role in study design, data collection and analysis, decision to publish, or preparation of the manuscript.

Conflict of Interest: SDG is Founder, President and CEO of Proteas Bioanalytics Inc., BioLabs at the Lundquist Institute, 1124 West Carson Street, Torrance, CA 90502, USA.

798 # TABLE

Up-regulated genes

GO TERM	BENJ. PVAL	COUNTS	ENRICHMENT	EXPECTED	DESCRIPTION
GO:0006351	7.31e-05	54/1882	21.68	2.40	Transcription, DNA-template
GO:0006357	5.04e-05	51/1805	20.79	2.45	Regulation of transcription from RNA polymerase
GO:0044212	9.82e-05	32/847	9.76	3.28	Transcription regulatory region DNA binding
GO:0006325	3.12e-03	26/614	7.07	3.68	Chromatin organization
GO:0009653	1.65e-03	52/2069	23.86	2.18	Anatomical structure morphogenesis

Down-regulated genes

GO TERM	BENJ. PVAL	COUNTS	ENRICHMENT	EXPECTED	DESCRIPTION
GO:0045202	3.09e-08	36/905	8.99	4.01	Synapse
GO:0043005	1.10e-05	39/1285	12.76	3.06	Neuron projection
GO:0098793	4.23e-04	18/354	3.51	5.12	Presynapse
GO:0070382	1.02e-03	13/185	1.84	7.08	Exocytic vesicle
GO:0008021	2.64e-03	12/167	1.66	7.24	Synaptic vesicle
GO:0070044	1.04e-03	4/5	0.05	80.58	Synaptobrevin 2-SNAP-25-syntaxib-1a complex
GO:0031201	1.96e-01	6/49	0.49	12.33	SNARE complex
GO:0001505	1.13e-02	12/191	1.90	6.33	Regulation of neurotransmitter levels
GO:0061025	6.36e-02	10/151	1.50	6.67	Membrane fusion
GO:0051648	6.78e-02	11/188	1.87	5.89	Vesicle localisation

799

800 **Table 1: GO enrichment analyses of the up- and down-regulated genes expressed in the**

801 ***Dyrk1a*$^{C/C}$ hippocampus (*Benjamini* cut-off of P < 0.05).**

802

Figure Legends

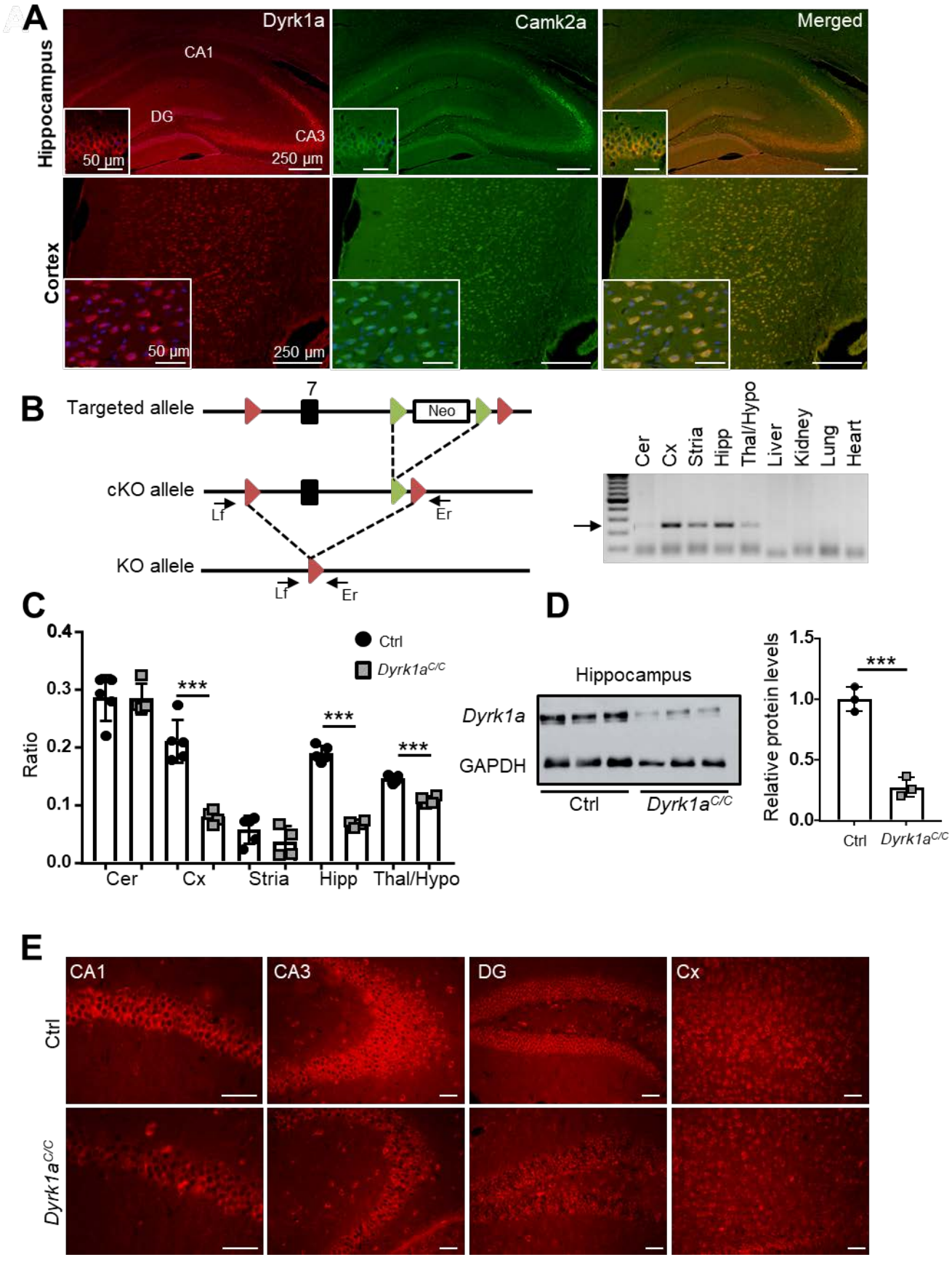

Figure 1: Generation of mice deficient for Dyrk1a in the glutamatergic neurons. (A) DYRK1A (red) co-localizes with CAMK2A (green) in the glutamatergic pyramidal neurons of the CA1-3, the granular neurons of the dentate gyrus (DG) and in the cortex. (B) Targeting strategy for conditional inactivation of *Dyrk1a*. Exon 7 containing the serine/threonine protein kinase active site was flanked with loxP sites (red arrowheads) in two steps: a targeted allele was first generated by homologous recombination in ES cells, then *in vivo* expression of the Flp recombinase resulted in recombinaison of the FRT sites (green arrowheads) and removal of the selection cassette (white box) generating the conditional allele (cKO). The knock-out allele (KO) was observed in the brain of *Dyrk1a*$^{C/C}$. Arrows represent primers for PCR genotyping. Genomic DNA was isolated from different organs from a *Dyrk1a*$^{C/C}$ mouse and genotyped for the presence of the knock-out allele with primers Lf and Er, giving a 232 bp PCR product for the KO allele. (C) Ratio of relative mRNA of *Dyrk1a* in different brain structures in *Dyrk1a*$^{C/C}$ and disomic control mice. (D) Autoradiographic image and quantification of immunoblots of DYRK1A protein in the hippocampus of *Dyrk1a*$^{C/C}$ mice relative to control mice. Band intensities were estimated using ImageJ and normalized against the loading control GAPDH. (E) DYRK1A immunohistochemistry of coronal brain sections at the level of the hippocampus from control and *Dyrk1a*$^{C/C}$ mice. Data are presented as point plots with mean ± SD with unpaired Student's t-test, *p<0.05, **p<0.01, ***p<0.001 (n=5 ctrl and 4 *Dyrk1a*$^{C/C}$ hippocampus for mRNA analysis and n=3 per genotype for protein analysis). CA1, Cornus Ammonis 1; CA3, Cornus Ammonis 3; DG, Dentate Gyrus; Cer: Cerebellum; Cx, Cortex.

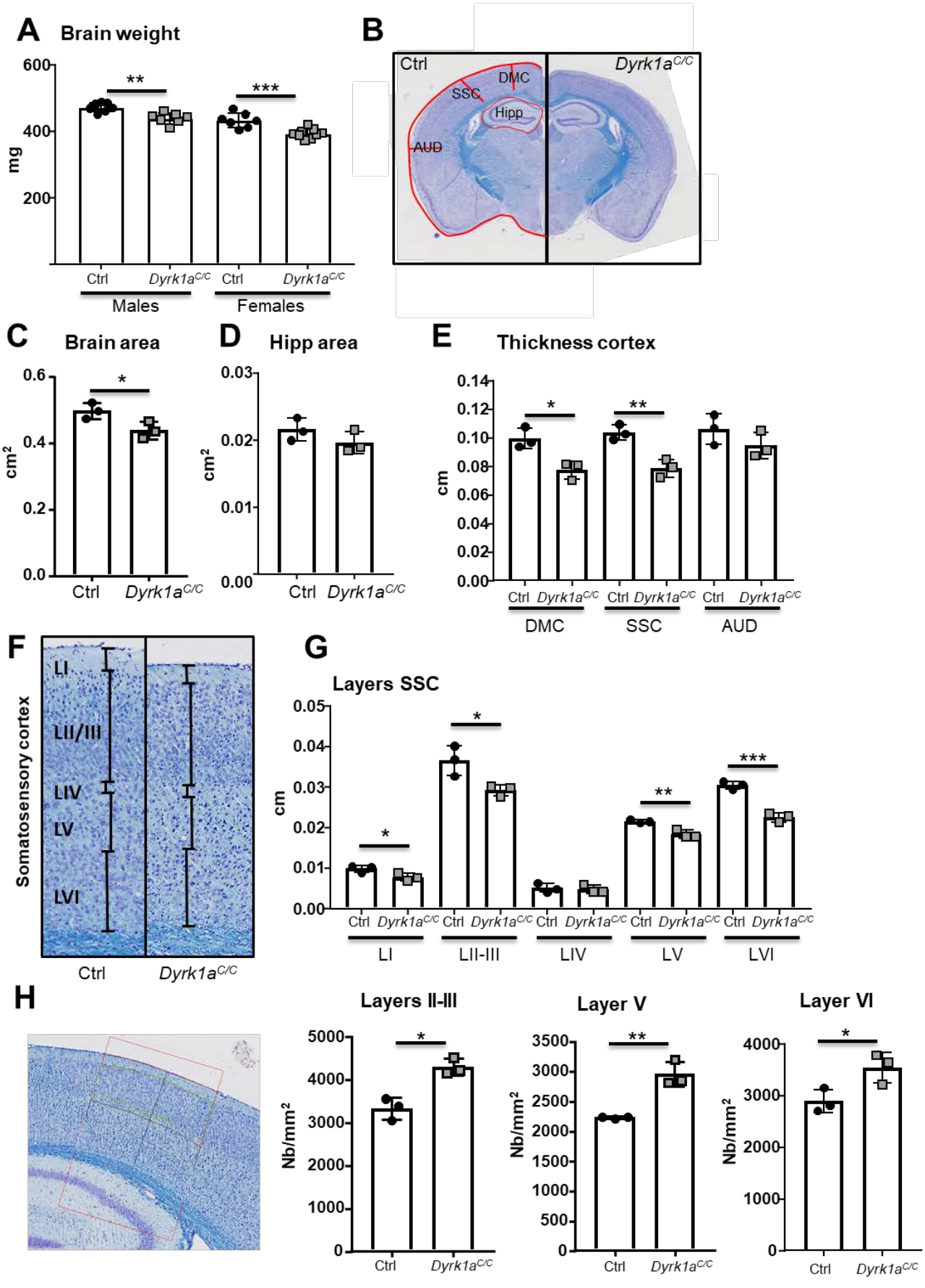

827 **Figure 2: Consequence of *Dyrk1a* inactivation in glutamatergic neurons on brain**
828 **morphology.** (A) Brain weight from male and female mice aged 3 months old (n=7-9 per
829 genotype). (B) Representative coronal sections of control (Ctrl) (left) and *Dyrk1a*$^{C/C}$ (right)
830 brains at Bregma -1.5 stained with cresyl violet and luxol blue that were used for measurements
831 (Magnification 20X). (C) Dot plots of total brain area measurements (red line around the brain
832 in B). (D) Dot plots of hippocampal areas (red area around hipp in B). (E) Measurements of the
833 thickness of the cortex at the 3 levels represented by red lines in figure B. (F) Representative
834 cresyl violet and luxol blue stained coronal sections of somatosensory cortex layers in control
835 (ctrl) and *Dyrk1a*$^{C/C}$ brains at Bregma -1.5. (G) Measurements of the thickness of the different
836 layers presented in figure F. (H) Relative density of cells counted in layers II-III, V and VI
837 within a frame of 0.1 cm width (see figure) at the level of the somatosensory cortex. Data are
838 presented as point plots with mean ± SD with unpaired Student's t-test, *p<0.05, **p<0.01,
839 ***p<0.001 (n=3 females per genotype). AUD: auditory cortex, SSC: somatosensory cortex,
840 DMC: dorso motor cortex, Hipp: hippocampus.
841

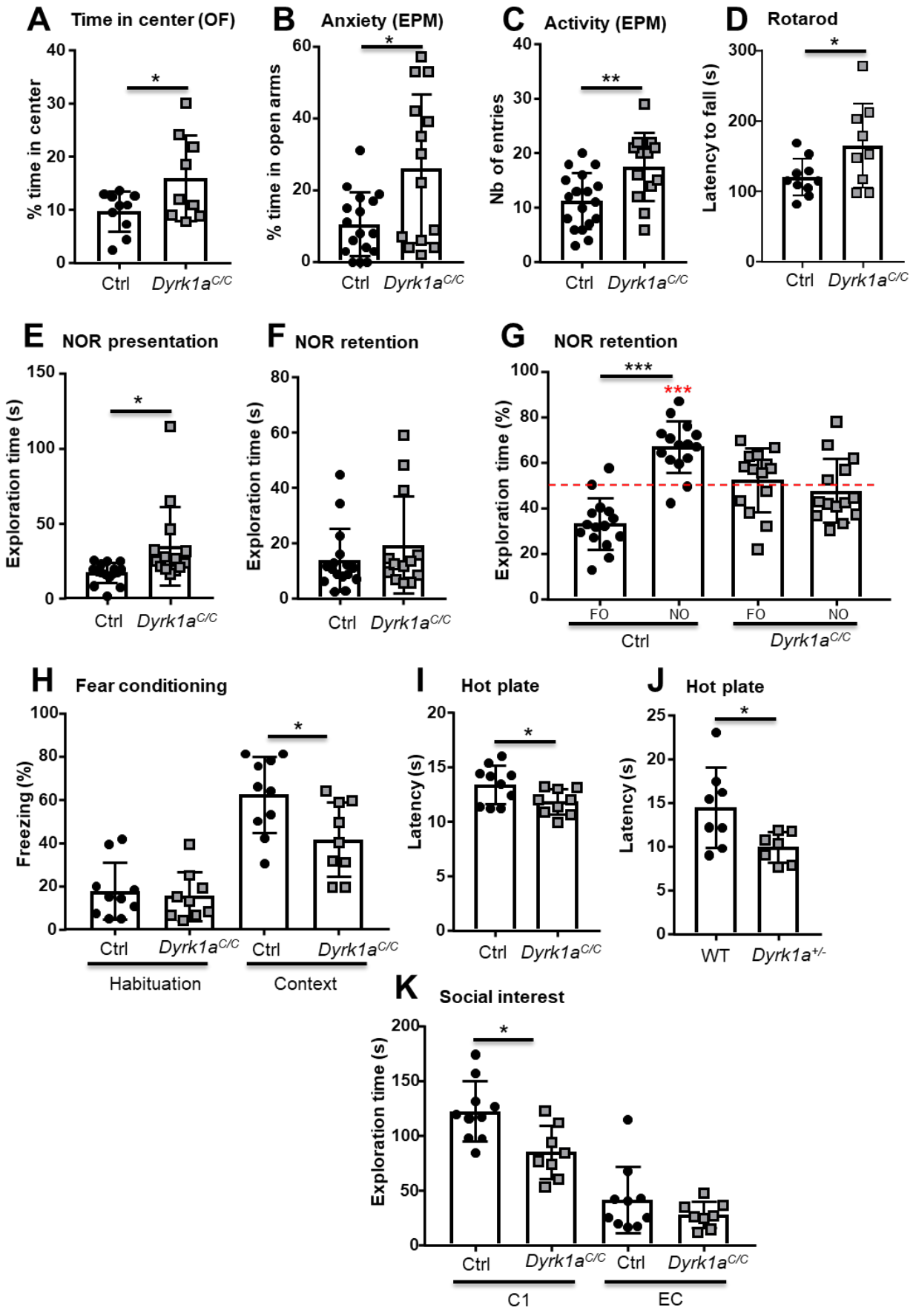

Figure 3: Impact of *Dyrk1a* inactivation in glutamatergic neurons on general behavior, locomotor activity and cognition. (A) The exploratory behavior of a new environment was analyzed by the percentage of time spent in the center of an open field over 30 min of test. *Dyrk1a*$^{C/C}$ mice spent more time in the center of the arena, suggesting that they are less anxious. (B) Confirmation of the phenotype in a new group of mice using the Elevated Plus Maze test (EPM) with *Dyrk1a*$^{C/C}$ mice showing a higher percentage of time spent in the open arms of the maze. (C) Mouse activity, measured by the number of entries in both open and closed arms, was increased in *Dyrk1a*$^{C/C}$ animals. (D) Evaluation of the locomotor performance on the rotarod during consecutive trials with increased rotational speeds. The latency is the mean of 3 independent trials. *Dyrk1a*$^{C/C}$ mice showed increased performance. (E) In the NOR test, the percentage of time spent exploring the familiar (FO) and the new (NO) objects show that control mice spend significantly more time on the NO while *Dyrk1a*$^{C/C}$ mice do not make any difference between the two objects. (F) Exploration times of the two identical objects during the presentation phase of the NOR show that *Dyrk1a*$^{C/C}$ mice tend to have an increased exploration time. (G) Total exploratory time of the two objects during the test indicates that the absence of object discrimination of the *Dyrk1a*$^{C/C}$ mice is not due to a lack of interest of the objects. (H) Percentage of freezing time during the habituation phase (before the foot shock; basal level of activity) (Habituation; Mann-Whitney rank sum test, p=0.71) and during the 6 min of contextual exposure 24 hours later indicate a deficit of contextual learning in *Dyrk1a*$^{C/C}$ mice. (I-J) Pain sensitivity was evaluated by measuring the mouse latency to elicit a response to pain when put on a plate (52°C). In this test, *Dyrk1a*$^{C/C}$ and *Dyrk1a*$^{+/-}$ mice had a lower threshold than their control littermates. (K) Interest in social interaction was measured by the time spent sniffing the cage containing a congener (C1) during the Crawley test. This time was reduced for *Dyrk1a*$^{C/C}$ mice compared to control mice (unpaired t-test p=0.01) while the time spent exploring the empty cage (EC) was the same between the two groups (unpaired t-test p=0.23).

Data are presented as point plots with mean ± SD. Statistical analyses were done with unpaired Student's t-test or Mann-Whitney rank sum test if normality test failed, except E: paired T-test FO vs NO and one sample T-test vs 50% mean (in red: ***p<0.001); n=8-10 per genotype. B-C (EPM) and E-G (NOR) were done with another batch of mice, n=14-15 per genotype; *p<0.05, **p<0.01, ***p<0.001.

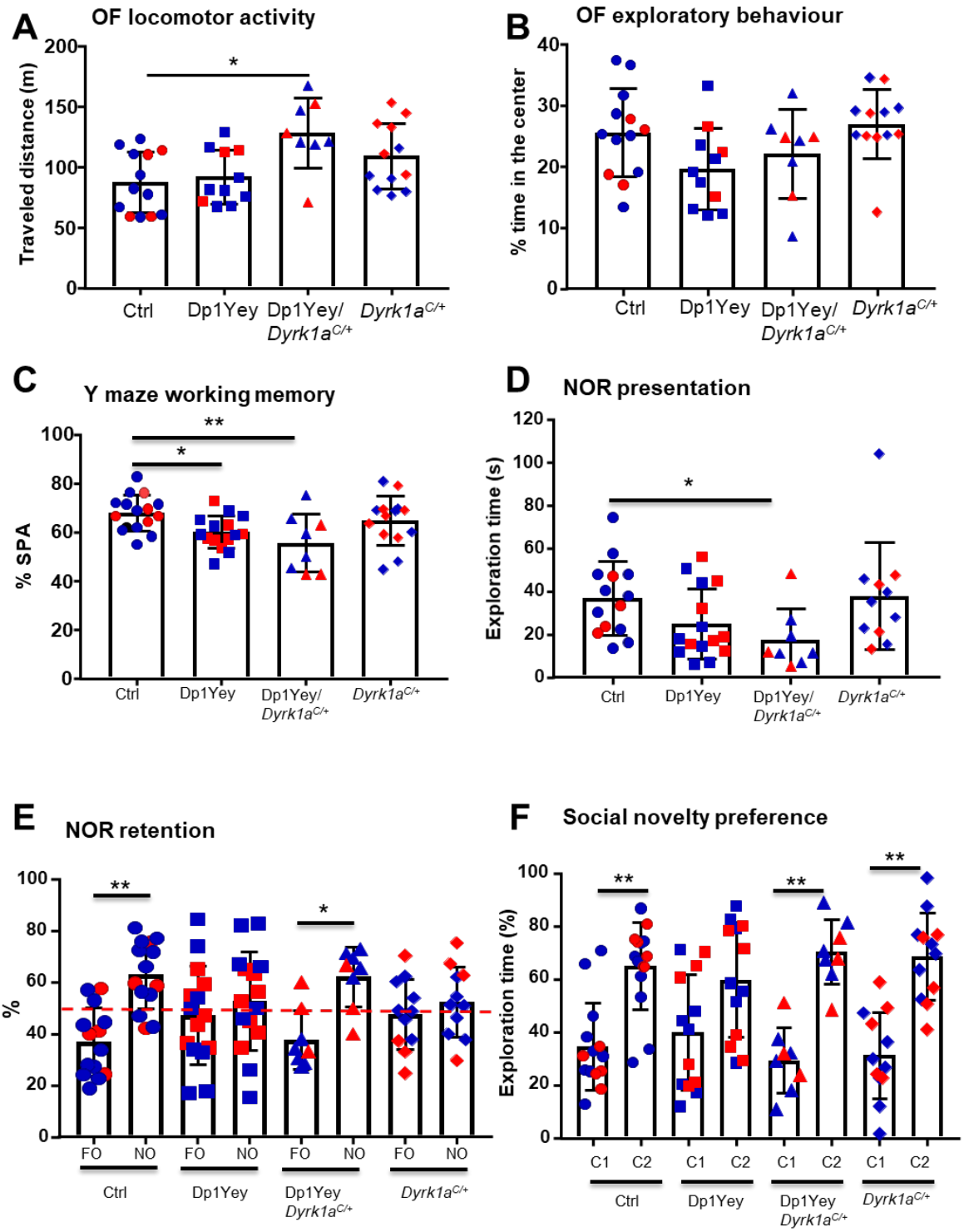

Figure 4: Consequence of the normalization of *Dyrk1a* in glutamatergic neurons of Dp1Yey mice on animal cognition. (A) The total distance travelled in the open field during a 30 min session is significantly increased in the Dp1Yey/*Dyrk1a*$^{C/+}$ mice compared to the control mice (Kruskal-Wallis One Way Analysis of Variance on Ranks, p=0.009 with Dunn's post hoc multiple comparison procedures versus control, Dp1Yey/*Dyrk1*$^{C//+}$ vs control, p=0.007). (B) Percentage time spent in the center of the OF does not vary between genotypes (One way ANOVA, F(3, 40)=2.76, p=0.054). (C) Percentage of spontaneous alternation of the mice during a 5 min session in a Y-maze. Lower percentage of alternation was found in Dp1Yey mice and in Dp1Yey/*Dyrk1a*$^{C/+}$ indicating a deficit in working memory in Dp1Yey mice that is not rescued in Dp1Yey/*Dyrk1a*$^{C/+}$ mice (One way ANOVA, Holm-Sidak method for multiple comparisons versus control group, F(3,49)=4.3, p=0.009, Dp1Yey vs control q=2.48, p=0.03, Dp1Yey/*Dyrk1a*$^{C/+}$ q=3.24, p=0.006). (D-E) Novel object recognition was assessed with 24 hour time laps. (D) Time spent exploring the two identical objects during the first object presentation session was decreased in Dp1Yey/*Dyrk1a*$^{C/+}$ mice (Kruskal-Wallis One Way Analysis of Variance on Ranks, p=0.02 with Dunn's post hoc multiple comparison procedures versus control, Dp1Yey/*Dyrk1a*$^{C//+}$ vs control, p=0.02). (E) When introducing the novel object during the retention period, both control and Dp1Yey/*Dyrk1a*$^{C/+}$ lines spent significantly more time exploring the novel object than the familiar one (Paired t-test novel object vs familiar object, ctrl p=0.003, Dp1Yey/*Dyrk1a*$^{C/+}$ p=0.02), whereas *Dp1Yey* and *Dyrk1a*$^{C/+}$ mice did not (Paired t-test novel object vs familiar object, Dp1Yey p=0.57, *Dyrk1a*$^{C/+}$ p=0.56), revealing a significant deficit in memory for both Dp1Yey and *Dyrk1a*$^{C/+}$ mice which is rescued in Dp1Yey/*Dyrk1a*$^{C/+}$ mice. (F) Mice were tested for social novelty preference. All the genotypes but Dp1Yey spent significantly more time sniffing the new congener (Paired t-test congener vs empty cage, ctrl p=0.004, Dp1Yey p=0.13, Dp1Yey/*Dyrk1a*$^{C/+}$ p=0.002, *Dyrk1a*$^{C/+}$ p=0.002). Data are presented as point plots with mean ± SD. (n=8-15 per genotype, *p<0.05, **p<0.01)

899 Males (in blue) and females (in red) are pooled in the same graph as the statistical analyses did

900 not reveal significant effect of sex.

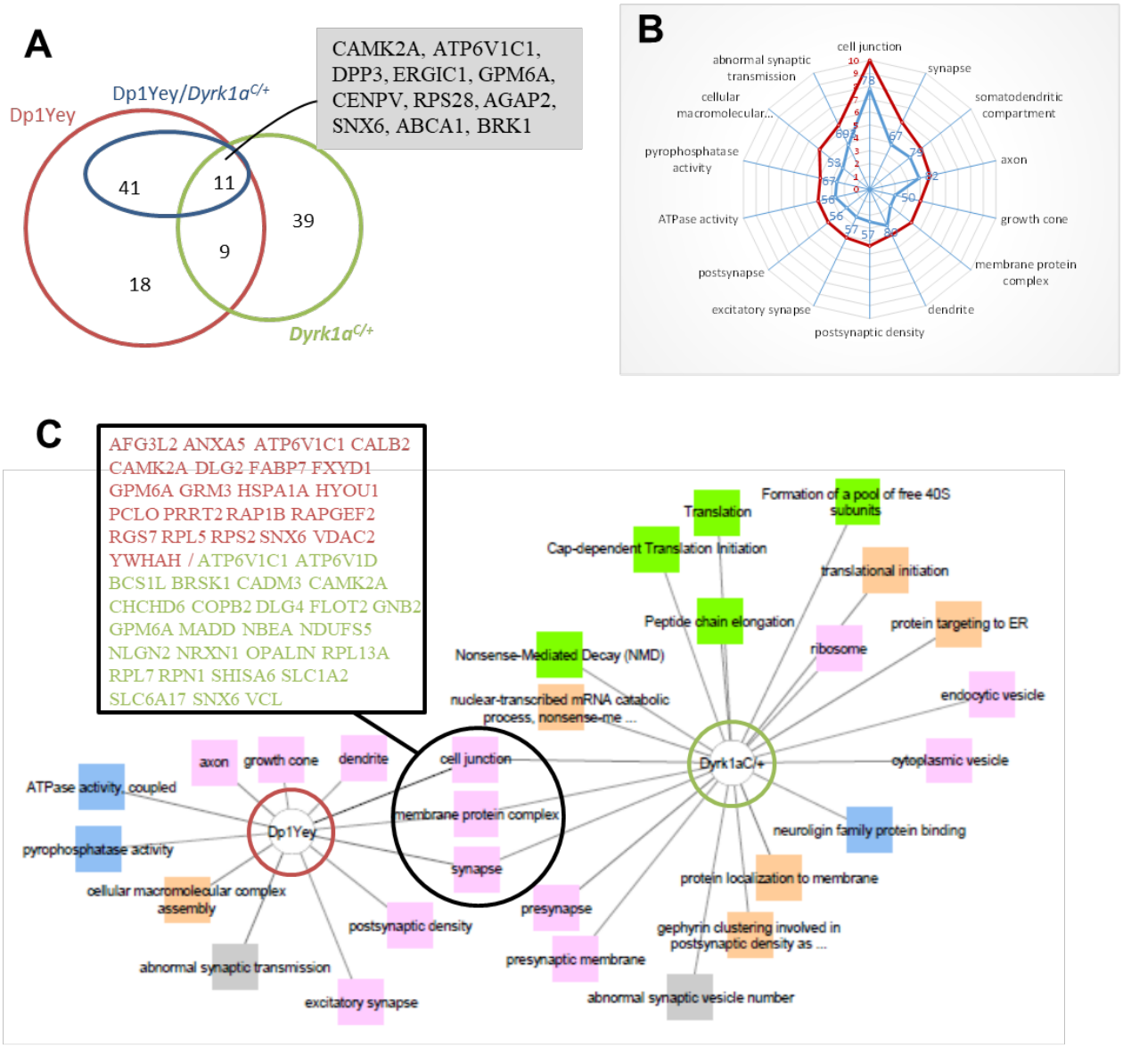

901

902

Figure 5: Proteomic analysis (A) Venn diagram showing the numbers of deregulated proteins in the different mouse models. The numbers of proteins shown for the Dp1Yey/*Dyrk1a*$^{C/+}$ model (in dark blue) correspond to proteins that were deregulated in the Dp1Yey and back to normal levels in this model (proteins that are regulated by Dyrk1a in the trisomy). Proteins deregulated by both *Dyrk1a* up and down-regulation (common to Dp1Yey, Dp1Yey/*Dyrk1a*$^{C/+}$ and *Dyrk1a*$^{C/+}$) are listed in the grey shaded box. (B) Radar plots of GO terms that are mostly enriched in the Dp1Yey model (in red with scale bar corresponding to the log of the p-value) and of the proportion of the proteins found deregulated in Dp1Yey which amount is normalized by the return in 2 copies in the Dp1Yey/*Dyrk1a*$^{C/+}$ model (in blue with scale bar corresponding to the % of Dp1Yey deregulated protein back to normal levels). (C) Visual representation of the GO enrichments for the deregulated proteins in Dp1Yey and *Dyrk1a*$^{C/+}$ hippocampi with connection between common terms. The different categories of GO are represented by different colors: pink for Cellular components", blue for "Molecular functions", green for "Pathways", orange for "Biological processes" and grey for "Phenotypes". The list of proteins in the box corresponds to proteins present in the common deregulated GO terms (in red deregulated proteins in Dp1Yey and in green proteins deregulated in *Dyrk1a*$^{C/+}$). (D) Western blots of DYRK1A, NR2B, PSD95, SYNGAP and CAMK2 proteins following IPs of wild-type mice brain extracts. We found in NR2B, PSD95 and CAMK2 in the IPs of DYRK1A. We also detected DYRK1A in the IPs of NR2B, PSD95 and SYNGAP.

References

1. Duchon A, Herault Y. DYRK1A, a Dosage-Sensitive Gene Involved in Neurodevelopmental Disorders, Is a Target for Drug Development in Down Syndrome. Front Behav Neurosci. 2016;10:104. Epub 2016/06/03. doi: 10.3389/fnbeh.2016.00104. PubMed PMID: 27375444; PubMed Central PMCID: PMCPMC4891327.

2. Moller RS, Kuebart S, Hoeltzenbein M, Heye B, Vogel I, Hansen CP, et al. Truncation of the Down syndrome candidate gene DYRK1A in two unrelated patients with microcephaly.

931 American Journal of Human Genetics. 2008;82(5):1165-70. doi: 10.1016/j.ajhg.2008.03.001.
932 PubMed PMID: WOS:000255923600016.
933 3. Fujita H, Torii C, Kosaki R, Yamaguchi S, Kudoh J, Hayashi K, et al. Microdeletion of
934 the Down Syndrome Critical Region at 21q22. American Journal of Medical Genetics Part A.
935 2010;152A(4):950-3. doi: 10.1002/ajmg.a.33228. PubMed PMID: WOS:000276754000023.
936 4. Yamamoto T, Shimojima K, Nishizawa T, Matsuo M, Ito M, Imai K. Clinical
937 Manifestations of the Deletion of Down Syndrome Critical Region Including DYRK1A and
938 KCNJ6. American Journal of Medical Genetics Part A. 2011;155A(1):113-9. doi:
939 10.1002/ajmg.a.33735. PubMed PMID: WOS:000285889100015.
940 5. Valetto A, Orsini A, Bertini V, Toschi B, Bonuccelli A, Simi F, et al. Molecular
941 cytogenetic characterization of an interstitial deletion of chromosome 21 (21q22.13q22.3) in a
942 patient with dysmorphic features, intellectual disability and severe generalized epilepsy.
943 European Journal of Medical Genetics. 2012;55(5):362-6. doi: 10.1016/j.ejmg.2012.03.011.
944 PubMed PMID: WOS:000307540100015.
945 6. Bronicki LM, Redin C, Drunat S, Piton A, Lyons M, Passemard S, et al. Ten new cases
946 further delineate the syndromic intellectual disability phenotype caused by mutations in
947 DYRK1A. Eur J Hum Genet. 2015;23(11):1482-7. Epub 2015/04/29. doi:
948 10.1038/ejhg.2015.29. PubMed PMID: 25920557; PubMed Central PMCID:
949 PMCPMC4613470.
950 7. Ji JL, Lee H, Argiropoulos B, Dorrani N, Mann J, Martinez-Agosto JA, et al. DYRK1A
951 haploinsufficiency causes a new recognizable syndrome with microcephaly, intellectual
952 disability, speech impairment, and distinct facies. European Journal of Human Genetics.
953 2015;23(11):1473-81. doi: 10.1038/ejhg.2015.71. PubMed PMID: WOS:000362916200010.
954 8. Arron JR, Winslow MM, Polleri A, Chang CP, Wu H, Gao X, et al. NFAT dysregulation
955 by increased dosage of DSCR1 and DYRK1A on chromosome 21. Nature.
956 2006;441(7093):595-600. Epub 2006/03/22. doi: 10.1038/nature04678. PubMed PMID:
957 16554754.
958 9. Soppa U, Schumacher J, Florencio Ortiz V, Pasqualon T, Tejedor FJ, Becker W. The
959 Down syndrome-related protein kinase DYRK1A phosphorylates p27(Kip1) and Cyclin D1 and
960 induces cell cycle exit and neuronal differentiation. Cell Cycle. 2014;13(13):2084-100. Epub
961 2014/05/07. doi: 10.4161/cc.29104. PubMed PMID: 24806449; PubMed Central PMCID:
962 PMCPMC4111700.
963 10. Ahn KJ, Jeong HK, Choi HS, Ryoo SR, Kim YJ, Goo JS, et al. DYRK1A BAC
964 transgenic mice show altered synaptic plasticity with learning and memory defects. Neurobiol
965 Dis. 2006;22(3):463-72. Epub 2006/02/07. doi: 10.1016/j.nbd.2005.12.006. PubMed PMID:
966 16455265.
967 11. Altafaj X, Dierssen M, Baamonde C, Martí E, Visa J, Guimerà J, et al.
968 Neurodevelopmental delay, motor abnormalities and cognitive deficits in transgenic mice
969 overexpressing Dyrk1A (minibrain), a murine model of Down's syndrome. Hum Mol Genet.
970 2001;10(18):1915-23. PubMed PMID: 11555628.
971 12. Arqué G, Fotaki V, Fernández D, Martínez de Lagrán M, Arbonés ML, Dierssen M.
972 Impaired spatial learning strategies and novel object recognition in mice haploinsufficient for
973 the dual specificity tyrosine-regulated kinase-1A (Dyrk1A). PLoS One. 2008;3(7):e2575. Epub
974 2008/07/02. doi: 10.1371/journal.pone.0002575. PubMed PMID: 18648535; PubMed Central
975 PMCID: PMCPMC2481280.
976 13. Kleschevnikov AM, Belichenko PV, Villar AJ, Epstein CJ, Malenka RC, Mobley WC.
977 Hippocampal long-term potentiation suppressed by increased inhibition in the Ts65Dn mouse,
978 a genetic model of Down syndrome. J Neurosci. 2004;24(37):8153-60. doi:
979 10.1523/JNEUROSCI.1766-04.2004. PubMed PMID: 15371516.

14. Siarey RJ, Carlson EJ, Epstein CJ, Balbo A, Rapoport SI, Galdzicki Z. Increased synaptic depression in the Ts65Dn mouse, a model for mental retardation in Down syndrome. Neuropharmacology. 1999;38(12):1917-20. doi: 10.1016/s0028-3908(99)00083-0. PubMed PMID: WOS:000083790900012.

15. Boada R, Hutaff-Lee C, Schrader A, Weitzenkamp D, Benke TA, Goldson EJ, et al. Antagonism of NMDA receptors as a potential treatment for Down syndrome: a pilot randomized controlled trial. Translational Psychiatry. 2012;2. doi: 10.1038/tp.2012.66. PubMed PMID: WOS:000209337200002.

16. Cramer N, Galdzicki Z. From Abnormal Hippocampal Synaptic Plasticity in Down Syndrome Mouse Models to Cognitive Disability in Down Syndrome. Neural Plasticity. 2012;2012. doi: 10.1155/2012/101542. PubMed PMID: WOS:000307581200001.

17. García-Cerro S, Martínez P, Vidal V, Corrales A, Flórez J, Vidal R, et al. Overexpression of Dyrk1A is implicated in several cognitive, electrophysiological and neuromorphological alterations found in a mouse model of Down syndrome. PLoS One. 2014;9(9):e106572. Epub 2014/09/04. doi: 10.1371/journal.pone.0106572. PubMed PMID: 25188425; PubMed Central PMCID: PMCPMC4154723.

18. Altafaj X, Martín ED, Ortiz-Abalia J, Valderrama A, Lao-Peregrín C, Dierssen M, et al. Normalization of Dyrk1A expression by AAV2/1-shDyrk1A attenuates hippocampal-dependent defects in the Ts65Dn mouse model of Down syndrome. Neurobiol Dis. 2013;52:117-27. Epub 2012/12/05. doi: 10.1016/j.nbd.2012.11.017. PubMed PMID: 23220201.

19. Fotaki V, Dierssen M, Alcántara S, Martínez S, Martí E, Casas C, et al. Dyrk1A haploinsufficiency affects viability and causes developmental delay and abnormal brain morphology in mice. Mol Cell Biol. 2002;22(18):6636-47. PubMed PMID: 12192061; PubMed Central PMCID: PMCPMC135639.

20. Mantamadiotis T, Lemberger T, Bleckmann SC, Kern H, Kretz O, Martin Villalba A, et al. Disruption of CREB function in brain leads to neurodegeneration. Nat Genet. 2002;31(1):47-54. Epub 2002/04/22. doi: 10.1038/ng882. PubMed PMID: 11967539.

21. Duchon A, Raveau M, Chevalier C, Nalesso V, Sharp AJ, Herault Y. Identification of the translocation breakpoints in the Ts65Dn and Ts1Cje mouse lines: relevance for modeling down syndrome. Mammalian Genome. 2011;22(11-12):674-84. doi: 10.1007/s00335-011-9356-0. PubMed PMID: WOS:000297544700004.

22. Martí E, Altafaj X, Dierssen M, de la Luna S, Fotaki V, Alvarez M, et al. Dyrk1A expression pattern supports specific roles of this kinase in the adult central nervous system. Brain Res. 2003;964(2):250-63. PubMed PMID: 12576186.

23. Kinnavane L, Amin E, Olarte-Sanchez CM, Aggleton JP. Detecting and Discriminating Novel Objects: The Impact of Perirhinal Cortex Disconnection on Hippocampal Activity Patterns. Hippocampus. 2016;26(11):1393-413. doi: 10.1002/hipo.22615. PubMed PMID: WOS:000387590300003.

24. Bussey TJ, Saksidal LM. Memory, perception, and the ventral visual-perirhinal-hippocampal stream: Thinking outside of the boxes. Hippocampus. 2007;17(9):898-908. doi: 10.1002/hipo.20320. PubMed PMID: WOS:000249423700018.

25. Fernandez G, Tendolkar I. The rhinal cortex: 'gatekeeper' of the declarative memory system. Trends in Cognitive Sciences. 2006;10(8):358-62. doi: 10.1016/j.tics.2006.06.003. PubMed PMID: WOS:000240090900008.

26. Rozeske RR, Valerio S, Chaudun F, Herry C. Prefrontal neuronal circuits of contextual fear conditioning. Genes Brain and Behavior. 2015;14(1):22-36. doi: 10.1111/gbb.12181. PubMed PMID: WOS:000349030000003.

27. Spiegel I, Mardinly AR, Gabel HW, Bazinet JE, Couch CH, Tzeng CP, et al. Npas4 Regulates Excitatory-Inhibitory Balance within Neural Circuits through Cell-Type-Specific

Gene Programs. Cell. 2014;157(5):1216-29. doi: 10.1016/j.cell.2014.03.058. PubMed PMID: WOS:000336437200021.

28. Jiang X, Liu C, Yu T, Zhang L, Meng K, Xing Z, et al. Genetic dissection of the Down syndrome critical region. Hum Mol Genet. 2015;24(22):6540-51. Epub 2015/09/15. doi: 10.1093/hmg/ddv364. PubMed PMID: 26374847; PubMed Central PMCID: PMCPMC4614710.

29. Hilfiker S, Benfenati F, Doussau FDR, Nairn AC, Czernik AJ, Augustine GJ, et al. Structural domains involved in the regulation of transmitter release by synapsins. Journal of Neuroscience. 2005;25(10):2658-69. doi: 10.1523/jneurosci.4278-04.2005. PubMed PMID: WOS:000227528600025.

30. Benfenati F, Valtorta F, Greengard P. COMPUTER MODELING OF SYNAPSIN-I BINDING TO SYNAPTIC VESICLES AND F-ACTIN - IMPLICATIONS FOR REGULATION OF NEUROTRANSMITTER RELEASE. Proceedings of the National Academy of Sciences of the United States of America. 1991;88(2):575-9. doi: 10.1073/pnas.88.2.575. PubMed PMID: WOS:A1991ET52100054.

31. Llinas R, Gruner JA, Sugimori M, McGuinness TL, Greengard P. REGULATION BY SYNAPSIN-I AND CA2+-CALMODULIN-DEPENDENT PROTEIN-KINASE II OF TRANSMITTER RELEASE IN SQUID GIANT SYNAPSE. Journal of Physiology-London. 1991;436:257-82. doi: 10.1113/jphysiol.1991.sp018549. PubMed PMID: WOS:A1991FM06300015.

32. Cesca F, Baldelli P, Valtorta F, Benfenati F. The synapsins: Key actors of synapse function and plasticity. Progress in Neurobiology. 2010;91(4):313-48. doi: 10.1016/j.pneurobio.2010.04.006. PubMed PMID: WOS:000280321300004.

33. Nguyen TL, Duchon A, Manousopoulou A, Loaëc N, Villiers B, Pani G, et al. Correction of cognitive deficits in mouse models of Down syndrome by a pharmacological inhibitor of DYRK1A. Dis Model Mech. 2018;11(9). Epub 2018/09/27. doi: 10.1242/dmm.035634. PubMed PMID: 30115750; PubMed Central PMCID: PMCPMC6176987.

34. Fukunaga K, Muller D, Miyamoto E. CaM kinase II in long-term potentiation. Neurochemistry International. 1996;28(4):343-58. doi: 10.1016/0197-0186(95)00097-6. PubMed PMID: WOS:A1996UH93800001.

35. Guedj F, Pereira PL, Najas S, Barallobre MJ, Chabert C, Souchet B, et al. DYRK1A: a master regulatory protein controlling brain growth. Neurobiol Dis. 2012;46(1):190-203. Epub 2012/01/26. doi: 10.1016/j.nbd.2012.01.007. PubMed PMID: 22293606.

36. Benavides-Piccione R, Dierssen M, Ballesteros-Yáñez I, Martínez de Lagrán M, Arbonés ML, Fotaki V, et al. Alterations in the phenotype of neocortical pyramidal cells in the Dyrk1A+/- mouse. Neurobiol Dis. 2005;20(1):115-22. doi: 10.1016/j.nbd.2005.02.004. PubMed PMID: 16137572.

37. Dang T, Duan WY, Yu B, Tong DL, Cheng C, Zhang YF, et al. Autism-associated Dyrk1a truncation mutants impair neuronal dendritic and spine growth and interfere with postnatal cortical development. Mol Psychiatry. 2018;23(3):747-58. Epub 2017/02/07. doi: 10.1038/mp.2016.253. PubMed PMID: 28167836; PubMed Central PMCID: PMCPMC5822466.

38. Zhang CL, Houbaert X, Lepleux M, Deshors M, Normand E, Gambino F, et al. The hippocampo-amygdala control of contextual fear expression is affected in a model of intellectual disability. Brain Structure & Function. 2015;220(6):3673-82. doi: 10.1007/s00429-014-0882-x. PubMed PMID: WOS:000361566000037.

39. Fotaki V, Martínez De Lagrán M, Estivill X, Arbonés M, Dierssen M. Haploinsufficiency of Dyrk1A in mice leads to specific alterations in the development and

regulation of motor activity. Behav Neurosci. 2004;118(4):815-21. doi: 10.1037/0735-7044.118.4.815. PubMed PMID: 15301607.

40. Sawynok J, Liu XJ. Adenosine in the spinal cord and periphery: release and regulation of pain. Progress in Neurobiology. 2003;69(5):313-40. doi: 10.1016/s0301-0082(03)00050-9. PubMed PMID: WOS:000183596300002.

41. Braudeau J, Delatour B, Duchon A, Pereira PL, Dauphinot L, de Chaumont F, et al. Specific targeting of the GABA-A receptor alpha 5 subtype by a selective inverse agonist restores cognitive deficits in Down syndrome mice. Journal of Psychopharmacology. 2011;25(8):1030-42. doi: 10.1177/0269881111405366. PubMed PMID: WOS:000293756100003.

42. Dragunow M. A role for immediate-early transcription factors in learning and memory. Behavior Genetics. 1996;26(3):293-9. doi: 10.1007/bf02359385. PubMed PMID: WOS:A1996UU94600007.

43. Smith-Hicks CL, Cai P, Savonenko AV, Reeves RH, Worley PF. Increased Sparsity of Hippocampal CA1 Neuronal Ensembles in a Mouse Model of Down Syndrome Assayed by Arc Expression. Front Neural Circuits. 2017;11:6. Epub 2017/02/03. doi: 10.3389/fncir.2017.00006. PubMed PMID: 28217086; PubMed Central PMCID: PMCPMC5289947.

44. Murakami N, Xie W, Lu RC, Chen-Hwang MC, Wieraszko A, Hwang YW. Phosphorylation of amphiphysin I by minibrain kinase/dual-specificity tyrosine phosphorylation-regulated kinase, a kinase implicated in Down syndrome. Journal of Biological Chemistry. 2006;281(33):23712-24. doi: 10.1074/jbc.M513497200. PubMed PMID: WOS:000239702900046.

45. Park JH, Jung MS, Kim YS, Song WJ, Chung SH. Phosphorylation of Munc18-1 by Dyrk1A regulates its interaction with Syntaxin 1 and X11α. J Neurochem. 2012;122(5):1081-91. Epub 2012/08/03. doi: 10.1111/j.1471-4159.2012.07861.x. PubMed PMID: 22765017.

46. Chen-Hwang MC, Chen HR, Elzinga M, Hwang YW. Dynamin is a minibrain kinase/dual specificity Yak1-related kinase 1A substrate. Journal of Biological Chemistry. 2002;277(20):17597-604. doi: 10.1074/jbc.M111101200. PubMed PMID: WOS:000175685100028.

47. Adayev T, Chen-Hwang MC, Murakami N, Wang R, Hwang YW. MNB/DYRK1A phosphorylation regulates the interactions of synaptojanin 1 with endocytic accessory proteins. Biochemical and Biophysical Research Communications. 2006;351(4):1060-5. doi: 10.1016/j.bbrc.2006.10.169. PubMed PMID: WOS:000242425300043.

48. Alemany-Gonzalez M, Gener T, Nebot P, Vilademunt M, Dierssen M, Puig MV. Prefrontal-hippocampal functional connectivity encodes recognition memory and is impaired in intellectual disability. Proceedings of the National Academy of Sciences of the United States of America. 2020;117(21):11788-98. doi: 10.1073/pnas.1921314117. PubMed PMID: WOS:000536797100076.

49. Souchet B, Guedj F, Sahún I, Duchon A, Daubigney F, Badel A, et al. Excitation/inhibition balance and learning are modified by Dyrk1a gene dosage. Neurobiol Dis. 2014;69:65-75. Epub 2014/05/04. doi: 10.1016/j.nbd.2014.04.016. PubMed PMID: 24801365.

50. Souchet B, Guedj F, Penke-Verdier Z, Daubigney F, Duchon A, Herault Y, et al. Pharmacological correction of excitation/inhibition imbalance in Down syndrome mouse models. Front Behav Neurosci. 2015;9:267. Epub 2015/10/20. doi: 10.3389/fnbeh.2015.00267. PubMed PMID: 26539088; PubMed Central PMCID: PMCPMC4611057.

51. Yu T, Liu C, Belichenko P, Clapcote SJ, Li S, Pao A, et al. Effects of individual segmental trisomies of human chromosome 21 syntenic regions on hippocampal long-term potentiation and cognitive behaviors in mice. Brain Res. 2010;1366:162-71. Epub 2010/10/26.

1128 doi: 10.1016/j.brainres.2010.09.107. PubMed PMID: 20932954; PubMed Central PMCID:
1129 PMCPMC3027718.
1130 52. Lalonde R. The neurobiological basis of spontaneous alternation. Neuroscience and
1131 Biobehavioral Reviews. 2002;26(1):91-104. doi: 10.1016/s0149-7634(01)00041-0. PubMed
1132 PMID: WOS:000174286400009.
1133 53. Degroot A, Parent MB. Increasing acetylcholine levels in the hippocampus or entorhinal
1134 cortex reverses the impairing effects of septal GABA receptor activation on spontaneous
1135 alternation. Learning & Memory. 2000;7(5):293-302. doi: 10.1101/lm.32200. PubMed PMID:
1136 WOS:000168802100008.
1137 54. Parent MB, Laurey PT, Wilkniss S, Gold PE. Intraseptal infusions of muscimol impair
1138 spontaneous alternation performance: Infusions of glucose into the hippocampus, but not the
1139 medial septum, reverse the deficit. Neurobiology of Learning and Memory. 1997;68(1):75-85.
1140 doi: 10.1006/nlme.1997.3769. PubMed PMID: WOS:A1997XE32500009.
1141 55. Vicari S, Bellucci S, Carlesimo GA. Visual and spatial long-term memory: differential
1142 pattern of impairments in Williams and Down syndromes. Dev Med Child Neurol.
1143 2005;47(5):305-11. PubMed PMID: 15892372.
1144 56. Guedj F, Sebrie C, Rivals I, Ledru A, Paly E, Bizot JC, et al. Green Tea Polyphenols
1145 Rescue of Brain Defects Induced by Overexpression of DYRK1A. Plos One. 2009;4(2). doi:
1146 10.1371/journal.pone.0004606. PubMed PMID: WOS:000265487500011.
1147 57. De la Torre R, De Sola S, Pons M, Duchon A, de Lagran MM, Farre M, et al.
1148 Epigallocatechin-3-gallate, a DYRK1A inhibitor, rescues cognitive deficits in Down syndrome
1149 mouse models and in humans. Molecular Nutrition & Food Research. 2014;58(2):278-88. doi:
1150 10.1002/mnfr.201300325. PubMed PMID: WOS:000337629700007.
1151 58. Tasic B, Menon V, Nguyen TN, Kim TK, Jarsky T, Yao Z, et al. Adult mouse cortical
1152 cell taxonomy revealed by single cell transcriptomics. Nat Neurosci. 2016;19(2):335-46. Epub
1153 2016/01/04. doi: 10.1038/nn.4216. PubMed PMID: 26727548; PubMed Central PMCID:
1154 PMCPMC4985242.
1155 59. Altafaj X, Ortiz-Abalia J, Fernandez M, Potier MC, Laffaire J, Andreu N, et al.
1156 Increased NR2A expression and prolonged decay of NMDA-induced calcium transient in
1157 cerebellum of TgDyrk1A mice, a mouse model of Down syndrome. Neurobiology of Disease.
1158 2008;32(3):377-84. doi: 10.1016/j.nbd.2008.07.024. PubMed PMID: WOS:000261602500006.
1159 60. Kleschevnikov AM, Belichenko PV, Villar AJ, Epstein CJ, Malenka RC, Mobley WC.
1160 Hippocampal long-term potentiation suppressed by increased inhibition in the Ts65Dn mouse,
1161 a genetic model of Down syndrome. Journal of Neuroscience. 2004;24(37):8153-60. doi:
1162 10.1523/jneurosci.1766-04.2004. PubMed PMID: WOS:000223884400018.
1163 61. Best TK, Siarey RJ, Galdzicki Z. Ts65Dn, a mouse model of Down syndrome, exhibits
1164 increased GABAB-induced potassium current. J Neurophysiol. 2007;97(1):892-900. Epub
1165 2006/11/08. doi: 10.1152/jn.00626.2006. PubMed PMID: 17093127.
1166 62. Best TK, Cramer NP, Chakrabarti L, Haydar TF, Galdzicki Z. Dysfunctional
1167 hippocampal inhibition in the Ts65Dn mouse model of Down syndrome. Exp Neurol.
1168 2012;233(2):749-57. Epub 2011/12/08. doi: 10.1016/j.expneurol.2011.11.033. PubMed PMID:
1169 22178330; PubMed Central PMCID: PMCPMC4123861.
1170 63. Wu DF, Koch T, Liang YJ, Stumm R, Schulz S, Schröder H, et al. Membrane
1171 glycoprotein M6a interacts with the micro-opioid receptor and facilitates receptor endocytosis
1172 and recycling. J Biol Chem. 2007;282(30):22239-47. Epub 2007/06/04. doi:
1173 10.1074/jbc.M700941200. PubMed PMID: 17548356.
1174 64. Kim E, Cho KO, Rothschild A, Sheng M. Heteromultimerization and NMDA receptor-
1175 clustering activity of Chapsyn-110, a member of the PSD-95 family of proteins. Neuron.
1176 1996;17(1):103-13. doi: 10.1016/s0896-6273(00)80284-6. PubMed PMID: 8755482.

65. Camp AJ, Wijesinghe R. Calretinin: modulator of neuronal excitability. Int J Biochem Cell Biol. 2009;41(11):2118-21. Epub 2009/05/18. doi: 10.1016/j.biocel.2009.05.007. PubMed PMID: 19450707.
66. Gass N, Becker R, Sack M, Schwarz AJ, Reinwald J, Cosa-Linan A, et al. Antagonism at the NR2B subunit of NMDA receptors induces increased connectivity of the prefrontal and subcortical regions regulating reward behavior. Psychopharmacology. 2018;235(4):1055-68. doi: 10.1007/s00213-017-4823-2. PubMed PMID: WOS:000428421300011.
67. Wang DH, Jacobs SA, Tsien JZ. Targeting the NMDA receptor subunit NR2B for treating or preventing age-related memory decline. Expert Opinion on Therapeutic Targets. 2014;18(10):1121-30. doi: 10.1517/14728222.2014.941286. PubMed PMID: WOS:000342604900003.
68. Goebel DJ, Poosch MS. NMDA receptor subunit gene expression in the rat brain: a quantitative analysis of endogenous mRNA levels of NR1(Com), NR2A, NR2B, NR2C, NR2D and NR3A. Molecular Brain Research. 1999;69(2):164-70. PubMed PMID: WOS:000080836600002.
69. Cull-Candy S, Brickley S, Farrant M. NMDA receptor subunits: diversity, development and disease. Current Opinion in Neurobiology. 2001;11(3):327-35. doi: 10.1016/s0959-4388(00)00215-4. PubMed PMID: WOS:000169286200009.
70. Loftis JM, Janowsky A. The N-methyl-D-aspartate receptor subunit NR2B: localization, functional properties, regulation, and clinical implications. Pharmacology & Therapeutics. 2003;97(1):55-85. doi: 10.1016/s0163-7258(02)00302-9. PubMed PMID: WOS:000180383800003.
71. Liu LD, Wong TP, Pozza MF, Lingenhoehl K, Wang YS, Sheng M, et al. Role of NMDA receptor subtypes in governing the direction of hippocampal synaptic plasticity. Science. 2004;304(5673):1021-4. doi: 10.1126/science.1096615. PubMed PMID: WOS:000221383300052.
72. Fox CJ, Russell KI, Wang YT, Christie BR. Contribution of NR2A and NR2B NMDA subunits to bidirectional synaptic plasticity in the hippocampus in vivo. Hippocampus. 2006;16(11):907-15. doi: 10.1002/hipo.20230. PubMed PMID: WOS:000241833500001.
73. Bartlett TE, Bannister NJ, Collett VJ, Dargan SL, Massey PV, Bortolotto ZA, et al. Differential roles of NR2A and NR2B-containing NMDA receptors in LTP and LTD in the CA1 region of two-week old rat hippocampus. Neuropharmacology. 2007;52(1):60-70. doi: 10.1016/j.neuropharm.2006.07.013. PubMed PMID: WOS:000243698200007.
74. Grau C, Arato K, Fernandez-Fernandez JM, Valderrama A, Sindreu C, Fillat C, et al. DYRK1A-mediated phosphorylation of GluN2A at Ser(1048) regulates the surface expression and channel activity of GluN1/GluN2A receptors. Frontiers in Cellular Neuroscience. 2014;8. doi: 10.3389/fncel.2014.00331. PubMed PMID: WOS:000344534900001.
75. Li Z, Yu T, Morishima M, Pao A, LaDuca J, Conroy J, et al. Duplication of the entire 22.9 Mb human chromosome 21 syntenic region on mouse chromosome 16 causes cardiovascular and gastrointestinal abnormalities. Hum Mol Genet. 2007;16(11):1359-66. Epub 2007/04/05. doi: 10.1093/hmg/ddm086. PubMed PMID: 17412756.
76. Monory K, Massa F, Egertová M, Eder M, Blaudzun H, Westenbroek R, et al. The endocannabinoid system controls key epileptogenic circuits in the hippocampus. Neuron. 2006;51(4):455-66. doi: 10.1016/j.neuron.2006.07.006. PubMed PMID: 16908411; PubMed Central PMCID: PMCPMC1769341.
77. Rodriguez CI, Buchholz F, Galloway J, Sequerra R, Kasper J, Ayala R, et al. High-efficiency deleter mice show that FLPe is an alternative to Cre-loxP. Nature Genetics. 2000;25(2):139-40. doi: 10.1038/75973. PubMed PMID: WOS:000087459200007.
78. Jacquot S, Chartoire N, Piguet F, Hérault Y, Pavlovic G. Optimizing PCR for Mouse Genotyping: Recommendations for Reliable, Rapid, Cost Effective, Robust and Adaptable to

High-Throughput Genotyping Protocol for Any Type of Mutation. Curr Protoc Mouse Biol. 2019;9(4):e65. doi: 10.1002/cpmo.65. PubMed PMID: 31756054.

79. Lindner L, Cayrou P, Jacquot S, Birling MC, Herault Y, Pavlovic G. Reliable and robust droplet digital PCR (ddPCR) and RT-ddPCR protocols for mouse studies. Methods. 2020. Epub 2020/07/25. doi: 10.1016/j.ymeth.2020.07.004. PubMed PMID: 32721466.

80. Huggett JF, Group d. The Digital MIQE Guidelines Update: Minimum Information for Publication of Quantitative Digital PCR Experiments for 2020. Clin Chem. 2020;66(8):1012-29. doi: 10.1093/clinchem/hvaa125. PubMed PMID: 32746458.

81. Mikhaleva A, Kannan M, Wagner C, Yalcin B. Histomorphological Phenotyping of the Adult Mouse Brain. Curr Protoc Mouse Biol. 2016;6(3):307-32. Epub 2016/09/01. doi: 10.1002/cpmo.12. PubMed PMID: 27584555.

82. Dubos A, Meziane H, Iacono G, Curie A, Riet F, Martin C, et al. A new mouse model of ARX dup24 recapitulates the patients' behavioral and fine motor alterations. Hum Mol Genet. 2018;27(12):2138-53. doi: 10.1093/hmg/ddy122. PubMed PMID: 29659809; PubMed Central PMCID: PMCPMC5985730.

83. Arbogast T, Iacono G, Chevalier C, Afinowi NO, Houbaert X, van Eede MC, et al. Mouse models of 17q21.31 microdeletion and microduplication syndromes highlight the importance of Kansl1 for cognition. PLoS Genet. 2017;13(7):e1006886. Epub 2017/07/13. doi: 10.1371/journal.pgen.1006886. PubMed PMID: 28704368; PubMed Central PMCID: PMCPMC5531616.

84. Marechal D, Brault V, Leon A, Martin D, Lopes Pereira P, Loaëc N, et al. Cbs overdosage is necessary and sufficient to induce cognitive phenotypes in mouse models of Down syndrome and interacts genetically with Dyrk1a. Hum Mol Genet. 2019;28(9):1561-77. doi: 10.1093/hmg/ddy447. PubMed PMID: 30649339.